Editors' Suggestion

Edge-wave phase shifts versus normal-mode phase tilts in an Eady problem with a sloping boundary

J. Mak*
Department of Ocean Science, Hong Kong University of Science and Technology, Hong Kong and National Oceanography Centre, Southampton, United Kingdom

N. Harnik and E. Heifetz
Porter School of the Environment and Earth Sciences, Tel Aviv University, Tel Aviv 69978, Israel

G. Kumar†
Department of Mathematics, Faculty of Science and Technology (IcfaiTech), ICFAI Foundation for Higher Education, Hyderabad 501203, Telangana, India; Department of Ocean Science, Hong Kong University of Science and Technology, Hong Kong; and Center for Ocean Research in Hong Kong and Macau, Hong Kong University of Science and Technology, Hong Kong

E. Q. Y. Ong
Climate Change Research Centre, Australian Centre for Excellence in Antarctic Science, University of New South Wales, Sydney, NSW, Australia and Australian Research Council Centre of Excellence for Climate Extremes, University of New South Wales, Sydney, NSW, Australia

(Received 14 April 2024; accepted 24 July 2024; published 26 August 2024)

One mechanistic interpretation of baroclinic instability is that of mutual constructive interference of Rossby edge waves. The suppression of baroclinic instability over slopes has been widely established, where previous research argues that a sloping boundary modifies the properties of these Rossby edge waves, but does not provide a mechanistic explanation for the suppression that is valid over all parameter space. In the context of an Eady problem modified by the presence of a sloping boundary, we provide a mechanistic rationalization for baroclinic instability in the presence of slopes that is valid over all parameter space, via an equivalent formulation explicitly in terms of Rossby edge waves. We also highlight the differences between edge-wave phase shifts and normal-mode phase tilts, showing that the edge-wave phase shifts should be the ones that are mechanistically relevant, and normal-mode phase tilt is a potentially misleading quantity to use. Further, we present evidence that the edge-wave phase shifts but not normal-mode phase tilts are well correlated with geometric quantities diagnosed from an analysis framework based on eddy variance ellipses. The result is noteworthy in that the geometric framework makes no explicit reference to the edge-wave structures in its construction, and the correlation suggests the geometric

*Contact author: julian.c.l.mak@googlemail.com
†Contact author: gautam.kmr10@zohomail.in

framework can be used in problems where edge-wave structures are not so well defined or readily available. Some implications for parametrization of baroclinic instability and relevant eddy-mean feedbacks are discussed. For completeness, we also provide an explicit demonstration that the linear instability problem of the present modified Eady problem is parity-time symmetric, and speculate about some suggestive links between parity-time symmetry, shear instability, and the edge-wave interaction mechanism.

DOI: 10.1103/PhysRevFluids.9.083905

I. INTRODUCTION

Baroclinic dynamics and turbulence play a key role in rotating and stratified systems in the geophysical and astrophysical context, via the associated transport of buoyancy and impacts on the overturning circulation (e.g., [1–10]). Understanding the mechanisms and conditions for baroclinic instability, its transition to turbulence, and its eventual saturation is of interest in understanding and modeling of the evolution in the relevant rotating stratified systems, such as the Earth's ocean and atmosphere.

It is not too controversial to say the subject of baroclinic instability is rather well understood at least in the hydrodynamic regime, where the linear instability phase of idealized models has analytical solutions (e.g., [11–14]), and general stability theorems exist (e.g., [15–18]). The nonlinear evolution and equilibration can also be tackled, mostly by numerical means (e.g., [19–28]). Often of interest in those cases are the associated statistics such as meridional eddy buoyancy fluxes, which plays a role in the eddy-mean interaction in the relevant rotating stratified systems, and informs on the parametrization in numerical general circulation models. A link that has been of particular interest is that of *quasilinear control*, i.e., to what degree do the linear instability characteristics have an imprint on the nonlinear dynamics? While one could argue that the processes that are being parameterized are inherent manifestations of the nonlinear dynamics, and there is no strong reason that the relevant linear analysis should play any role, the fact remains that a relation does appear between the two (e.g., [29–33]). A piece of work of relevance here is the framework of [34,35] termed "Geometry and Energetics of Ocean Mesocale Eddies and Their Rectified Impact on Climate" (GEOMETRIC; see similar ideas from [36,37]). While the framework was motivated by parametrization of ocean mesoscale eddies, the GEOMETRIC framework highlights a link between the associated eddy fluxes in terms of geometric quantities associated with eddy variance ellipses (such as anisotropy factors and angles) and the linear instability properties in rotating stratified fluid dynamics. The scalings for turbulent transfer coefficients resulting from the analysis within the GEOMETRIC framework has found particular applicability in the parametrization of eddy buoyancy fluxes in numerical ocean general circulation models (e.g., [38–40]).

In the present case we are interested in the instability characteristics of baroclinic instability in the presence of a slope, where "slope" is broadly interpreted to mean a slope as a physical boundary (e.g., topography in the atmosphere and/or ocean), or motion in the presence of an impermeable surface arising from the relevant fluid properties (e.g., adiabatic flow above/below a sloping isentrope in planetary atmospheres, or magnetic field effects in the solar tachocline above the radiative zone). The focus here is of particular relevance in the field of oceanography, where the presence of continental slopes is generally seen to suppress eddy buoyancy fluxes over the slope regions (e.g., [41–58]), with consequences for the material exchange between the shelf and open ocean environment, and thus impacts on the associated physical circulation and/or marine ecology. One possible contributing factor for the observed suppression over slope regions is that the linear instability is itself suppressed and/or less efficient over regions with slopes (e.g., [41–45,47,53,54]). In relation to the GEOMETRIC parametrization, the work in [56] has found, by diagnoses of numerical simulation data, that a tuning parameter α normally interpreted as a baroclinic eddy efficiency for the feedback onto the mean state (e.g., [38]) is suppressed over the slope regions. A

slope suppressed α has been found to lead to improvements in idealized prognostic calculations [57], providing additional evidence that there should be reduced eddy feedback over slopes. The links between the observed suppression of this α parameter and possible links with linear stability analysis remain to be clarified.

Our main interest here is why exactly is baroclinic instability suppressed over slopes? An often invoked mechanism for baroclinic instability is the constructive interference of phase-locked Rossby edge waves, often termed the counterpropagating Rossby wave mechanism (e.g., [59–61]). Edge waves, in this case, are vertically trapped and can mutually constructively interfere by the nonlocal velocity arising from the local potential vorticity anomalies associated with the edge waves as they propagate along the background potential vorticity gradients. Existing works have either noted that the presence of a slope will lead to modification of the edge-wave properties but stopped short elaborating on what exactly is being modified (e.g., [43]), or considered the phase-speed matching as a simple criteria for phase locking of these edge waves (e.g., [47,53]). This work highlights that rationalizations solely based on phase-speed matching are overly simplified and incomplete, since they do not hold over all parameter space. We argue that phase-speed matching is a symptom of phase locking but, ultimately, is a manifestation from the combination of *counterpropagation against the mean flow* and *mutual interaction* between the edge waves, where edge waves can mutually amplify and affect each other's propagation depending on their phase difference. The mutual interaction aspect is part of the solution and should not be neglected, even if it makes the problem more intricate.

For the rationalization, we focus for concreteness on the Eady problem [12], modified by the presence of a bottom slope, motivated by the oceanic setup. The Eady problem is normally formulated in terms of the full-depth normal-mode streamfunction, which is generally a tilted structure in the vertical, and a key quantity often of interest is the associated *phase tilt*, which we define here to mean the phase difference between the maximum values of the streamfunction eigenfunction at the top and bottom boundary (e.g., [1,53]). However, given that we want to invoke dynamics of edge waves, it may seem out of place to present results that are manifestly not explicitly in terms of potential vorticity edge waves (although this is not uncommon in the literature). For this work, we reformulate the Eady problem explicitly in terms of potential vorticity edge waves to help with our mechanistic rationalization. A key quantity when dealing with edge waves is an associated *phase shift*, which we define here to mean the phase difference of the potential vorticity anomalies associated with the edge waves.

One thing we highlight in this work is that it is the *phase shifts* that are the features of dynamical relevance, while there is some misleading behavior associated with the *phase tilts*, and we advocate against the use of phase tilts, particularly when talking about the edge-wave interaction mechanism. We further support our arguments with an analysis of the modified Eady instability in terms of the GEOMETRIC framework. Motivated by the work of [62], which derives an explicit analytical relation between the interacting edge waves and the GEOMETRIC parameters but for a horizontal shear instability, we numerically diagnose quantities such as the eddy tilt angles and anisotropy parameters associated with the relevant eddy variance ellipses constructed from the normal-mode eigenfunction. We find a strong correlation between the edge-wave phase shift and the vertical eddy tilt angle (cf. the analogous result from [62] for a horizontal shear instability), while the eigenfunction phase tilt bears little resemblance or correlation to either of the aforementioned quantities. The suppression of the instability and eddy efficiency as invoked in parametrization of baroclinic eddies over bottom slopes is attributed principally to changes in the *buoyancy anisotropy* of the eddies. The link between GEOMETRIC and edge waves may be of further interest for analysis and parameterization: in cases where the edge waves are not well defined, it may in fact be useful to perform an analysis in the GEOMETRIC framework instead, while there are possibilities to use simplified reduced models of edge-wave interaction as a way to inform how various GEOMETRIC parameters may evolve if GEOMETRIC-based parametrizations are utilized.

The article is structured as follows. In Sec. II we provide a mathematical formulation of the modified Eady problem as well as an overview of the counterpropagating Rossby wave mechanism,

and present our arguments as to why we think the existing descriptions of the instability mechanism based on phase-speed matching are incomplete and overly simple. We additionally highlight that the modified Eady problem here is in fact parity-time ($\mathcal{PT}$) symmetric (e.g., [63–66]), which has consequences for the solution spectrum, but defer the expanded details and related discussion to the Appendix. To aid in our efforts towards an internally consistent rationalization for the Eady instability valid over all parameter space, we provide in Sec. III a rephrasing of the modified Eady problem explicitly in terms of edge waves (cf. [61,67]), with explicit references to the phase shift and asymmetry in the wave amplitude ratios. We provide evidence that the phase shifts are the physically relevant quantities, while the phase tilts from a standard analysis of the normal-mode eigenfunction can be misleading. We further provide evidence in Sec. IV with analysis of the modified Eady problem within the GEOMETRIC framework, demonstrating that there is a strong link between phase shifts and vertical eddy tilts, while the phase tilt resembles neither of those quantities. We summarize our results in Sec. V, and discuss some implications of our results for parametrization of baroclinic processes.

II. THE MODIFIED EADY PROBLEM AND THE COUNTERPROPAGATING ROSSBY WAVE MECHANISM

The Eady problem is one of the canonical examples for baroclinic instability (the others being the Phillips [13] and Charney-Green [11,14] problem). The instability mechanism in all these cases is often explained as a pair of phase-locked interacting counterpropagating Rossby waves that are constructively interfering (e.g., [1]), and the aforementioned cases differ by where the associated Rossby waves are located; in the Eady case, these are Rossby edge waves that are vertically trapped at the top and bottom boundaries. For concreteness, we focus on the Eady problem in this work, motivated by the oceanic problem. We first provide the mathematical formulation and an overview of the instability characteristic of the Eady problem in the presence of a bottom sloping boundary. In the second part, we provide an overview of the counterpropagating Rossby wave mechanism, recap the existing interpretations of how the mechanism is modified by the presence of a sloping boundary, and specify why we think the existing arguments are overly simplified and incomplete.

A. Mathematical formulation

The physical setup for the Eady problem is as illustrated in Fig. 1, for the Northern Hemisphere setting with Coriolis parameter $f_0 > 0$. For the side-on view presented in Fig. 1(a) where we assume the flow is in the zonal x direction, we have a linear flow in the vertical between two boundaries; in the atmospheric setting, the vertical boundaries could be thought of as the ground and the tropopause, while for the oceanic setting this could be thought of as the top and bottom of the ocean. We will elaborate on the waveforms drawn in Fig. 1(a) later. For the head-on view presented in Fig. 1(b), we consider the presence of a meridional slope, where the scale of variation in the meridional direction y is small and approximately linear. The setting drawn in Fig. 1(b) is such that a vortex tube is allowed to stretch more relative to the flat bottom case. The configuration could be thought of as adding to the bottom background potential vorticity, thus leading to a larger background potential vorticity gradient, and vice versa for the case where the bottom topography is tilted in the opposite sense.

We assume the dynamics is rotationally dominant (in the sense that the associated Rossby number is small) and can be described by the quasigeostrophic equations (e.g., [1]) formulated on a f plane, with potential vorticity advection in the interior, and quasigeostrophic buoyancy advection at the vertical surfaces. Mathematically, this is

$$\frac{\mathrm{D}q}{\mathrm{D}t} = 0, \quad z \in (H, -H_b), \qquad \frac{\mathrm{D}b}{\mathrm{D}t} = 0, \quad z = H, -H_b, \tag{1}$$

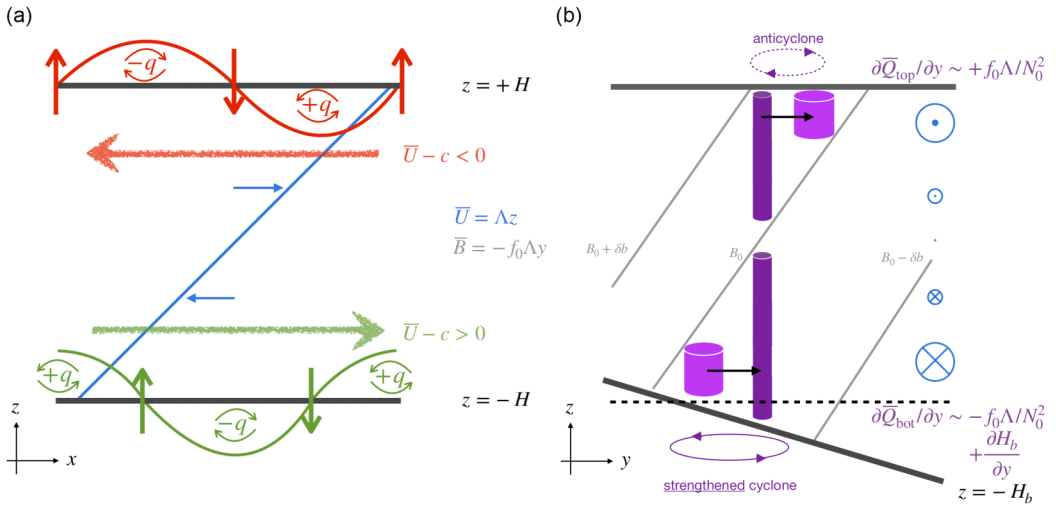

FIG. 1. Physical schematic for the current modified Eady problem. (a) Cross section of the setup, showing the basic state linear flow $\overline{U}$ in the zonal x direction, with Rossby edge waves drawn on at the vertical boundaries in an unstable configuration for a case where the interaction is symmetric (cf. a standard Eady problem, $\delta = 0$ here); see text for a description of the counterpropagating Rossby waves mechanism. (b) Head-on view, showing the basic state linear flow $\overline{U}$ going in and coming out of the page, and the associated buoyancy profile via thermal wind shear relation. The $\delta < 0$ case (topography and basic state buoyancy profile $\overline{B}$ at opposite orientations) is illustrated, where the contribution from the slope *reinforces* the bottom potential vorticity gradient by allowing extra stretching of a fluid column relative to the flat case, and can be unstable by the Charney-Stern-Pedlosky condition.

where the domain of interest is between $z = H$ and $z = -H_b(y)$, $H_b(y)$ represents the bottom slope, $\mathrm{D}/\mathrm{D}t = \partial/\partial t + \boldsymbol{u}\cdot\nabla$ is the material derivative, $\boldsymbol{u}$ is the (incompressible) geostrophic velocity with associated streamfunction ψ, ∇ is the horizontal gradient operator, and (x, y, z) denotes the zonal (east-west), meridional (north-south), and vertical coordinate. The potential vorticity q and quasigeostrophic buoyancy b are defined as

$$q = \nabla^2\psi + \frac{\partial}{\partial z}\frac{f_0}{N_0^2}b, \qquad b = f_0\frac{\partial\psi}{\partial z},$$

where $N_0^2 = \partial\overline{B}/\partial z$ is the buoyancy frequency associated with the prescribed background stratification, and $\overline{B}$ the basic state buoyancy profile to be prescribed with the basic state velocity $\overline{U}$. Contributions from the small slope will arise through the buoyancy equation in the advective term via $w = \boldsymbol{u}\cdot\nabla H_b$, arising from the no normal-flow condition on the bottom boundary.

We make an assumption that $\partial H_b(y)/\partial y$ is small [more precisely, that $(N_0/f_0)\partial H_b/\partial y$ is of order Rossby number, e.g., [43,53]], and that $\partial H_b(y)/\partial y$ can be approximated by a small constant contribution only in the boundary condition at $z = -H$. Then, linearizing against the basic state $\boldsymbol{u} = \overline{U}\boldsymbol{e}_x = \Lambda z\boldsymbol{e}_x$ (and so $\overline{B} = -f_0\Lambda y$ by the thermal wind shear relation), the governing linear equations are

$$\left(\frac{\partial}{\partial t} + \Lambda z\frac{\partial}{\partial x}\right)\left(\nabla^2\psi + \frac{f_0^2}{N_0^2}\frac{\partial^2\psi}{\partial z^2}\right) = 0, \quad z \in (-H, H), \tag{2a}$$

$$\left(\frac{\partial}{\partial t} + \Lambda H\frac{\partial}{\partial x}\right)\frac{\partial\psi}{\partial z} - \Lambda\frac{\partial\psi}{\partial x} = 0, \quad z = H, \tag{2b}$$

$$\left(\frac{\partial}{\partial t} - \Lambda H\frac{\partial}{\partial x}\right)\frac{\partial\psi}{\partial z} - \left(\Lambda - \frac{N_0^2}{f_0}\frac{\partial H_b}{\partial y}\right)\frac{\partial\psi}{\partial x} = 0, \quad z = -H. \tag{2c}$$

The Eady problem is constructed such that there is no background potential vorticity in the interior, hence the absence of a $\partial\overline{Q}/\partial y$ term. Nondimensionalizing by the horizontal length scale L, vertical length scale H, and timescale $T = L/U = L/(\Lambda H)$, we have

$$\left(\frac{\partial}{\partial t} + z\frac{\partial}{\partial x}\right)\left(\nabla^2\psi + F^2\frac{\partial^2\psi}{\partial z^2}\right) = 0, \quad z \in (-1, 1), \tag{3a}$$

$$\left(\frac{\partial}{\partial t} + \frac{\partial}{\partial x}\right)\frac{\partial\psi}{\partial z} - \frac{\partial\psi}{\partial x} = 0, \quad z = 1, \tag{3b}$$

$$\left(\frac{\partial}{\partial t} - \frac{\partial}{\partial x}\right)\frac{\partial\psi}{\partial z} - (1-\delta)\frac{\partial\psi}{\partial x} = 0, \quad z = -1, \tag{3c}$$

where $F^2 = (f_0 L/NH)^2$ and is the inverse of the Burgers number. A key nondimensional parameter in the present system is (in terms of dimensional variables)

$$\delta = \frac{\partial H_b}{\partial y}\left(\frac{N_0^2}{f_0\Lambda}\right) = \frac{\partial H_b}{\partial y}\Big/\frac{-\partial\overline{B}/\partial y}{\partial\overline{B}/\partial z} = \frac{\partial H_b/\partial y}{s}, \tag{4}$$

i.e., the parameter δ relates to the orientation of intersection between the background isopycnal slopes s with the bottom slope [a $\delta < 0$ case is illustrated in Fig. 1(b)]; this parameter is related to the α_T parameter in [47]. The cases $\delta < 0$ and $\delta > 0$ are sometimes known as retrograde or prograde configurations, although we will not be using that terminology here. One could relate the δ parameter here to a topographic β term, but we refer the reader to the work of [43] for that since we do not invoke that term in this work.

We make an observation that Eq. (3) is invariant under the transformation

$$\mathcal{P} : (x, y) \mapsto (-x, -y), \quad \mathcal{T} : (t, \psi) \mapsto (-t, -\psi), \tag{5}$$

so the system is parity-time ($\mathcal{PT}$) symmetric, where parity refers to a mirroring in space, while time symmetry refers to reversal of time [63–66]. Note that we regard δ as a given and prescribed parameter of the system, so δ does not transform under $\mathcal{P}$. The fact that the equations are $\mathcal{PT}$ symmetric implies the solution spectrum has certain properties [e.g., Figs. 2(b)–2(g)] and has very suggestive links for shear instabilities as well as the edge-wave interpretation; we refer the reader to the Appendix for details.

With appropriate horizontal boundary choices and conditions (periodic in the zonal x direction, periodic or appropriate no-normal flow boundary conditions in the meridional y direction), we consider solutions to Eq. (3) of the form

$$\psi(x, y, z, t) = \tilde{\psi}(z)\exp[\mathrm{i}(kx - \omega t)]g(y), \tag{6}$$

where $\tilde{\psi}$ is a vertical structure function in the streamfunction, $g(y)$ is an appropriate eigenfunction of the Laplacian operator so that $\partial^2 g/\partial y^2 = -l^2 g$ (e.g., combinations of $\sin ly$ and $\cos ly$ as appropriate), $\mathrm{i} = \sqrt{-1}$, (k, l) are the zonal and meridional wave numbers, $\omega = kc = k(c_r + \mathrm{i}c_i)$ is the angular frequency, and c is the (complex) phase speed; we have modal instability if $c_i > 0$. The vertical structure function satisfies

$$\tilde{\psi}(z) = a\cosh\mu z + b\sinh\mu z, \quad \mu^2 = (k^2 + l^2)/F^2. \tag{7}$$

The constants a and b are fixed by the compatibility condition resulting from the vertical boundary conditions. Making the shorthand $C = \cosh\mu$ and $S = \sinh\mu$, after some algebraic manipulation, the dispersion relation is given by

$$0 = c^2 + \frac{\delta}{2\mu}\left(\frac{C}{S} + \frac{S}{C}\right)c + \frac{\delta^2}{4\mu^2} - \left(\frac{1-\delta/2}{\mu} - \frac{C}{S}\right)\left(\frac{1-\delta/2}{\mu} - \frac{S}{C}\right). \tag{8}$$

Computing for c analytically or numerically, and denoting the solutions of the plus and minus branch as $c^{\pm}$ for ease of discussion, plots of $c_r^{\pm}$ and growth rate of the instability $kc_i^{\pm}$ as a function

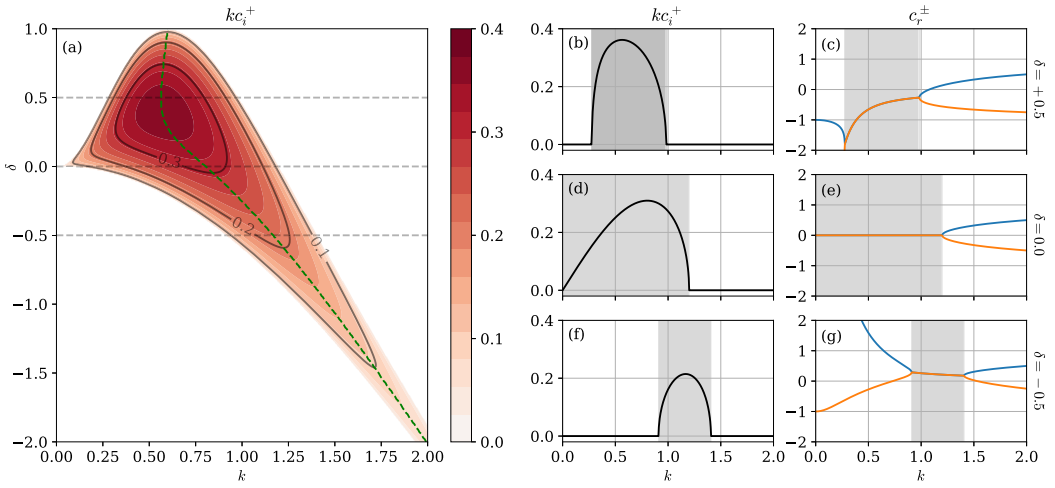

FIG. 2. General instability characteristics for the case of $l = 0$ (taking $F = 1$). (a) Growth rate as a function of the nondimensional zonal wave number k and δ parameter (as shading and sample contours), and the green dashed line denoting $k_{\max}(\delta)$ where the growth rate is maximized. Also shown are the growth rates kc_i^+ and phase speed $c_r^\pm$ for (b), (c) $\delta = +0.5$, (d), (e) the standard Eady problem $\delta = 0.0$, and (f), (g) $\delta = -0.5$. The shaded regions in panels (b)–(g) denote the regions where there the growth rates are nonzero.

of wave number k and δ can be constructed. It is generally known that the modes with the largest growth rates for a given parameter value are when the meridional wave number $l = 0$, i.e., two-dimensional modes, even if the nonlinear evolution is fundamentally three-dimensional (e.g., [1]). For the present work we will focus on the $l = 0$ case (with $F = 1$ for simplicity, which serves only as a scaling factor), and the general instability characteristic over (k, δ) parameter space is shown in Fig. 2. Note that, compared to more standard nondimensional formulations (e.g., [1,43,47,53]), our values of k and c are smaller and larger by a factor of 2 respectively, but kc_i remain the same.

A few features may be observed from Fig. 2:

(1) When $\delta = 0$ and there is instability, $c_r^\pm = 0$

(2) When $\delta \neq 0$ and there is instability, $c_r^+ = c_r^-$, and if $\delta > 0$, $c_r^\pm < 0$ (and vice versa for $\delta < 0$)

(3) There is no instability for $\delta \gtrsim 1$, but instability seems to persist for $\delta < 0$

(4) Relative to the standard $\delta = 0$ case, the most unstable wave number $k_{\max}$ decreases somewhat for $\delta > 0$, but persistently increases for $\delta < 0$, with the unstable bandwidth shifting to larger wave numbers.

The first point simply arises from our choice of problem formulation, where our domain goes from $z = \pm 1$ and our velocity profile is antisymmetric about $z = 0$ [cf. $c_r^\pm = (\overline{U}_{\text{top}} + \overline{U}_{\text{bot}})/2 = 0.5$ with the more standard formulations and choice of nondimensionalization in other works, e.g., [1,43,47,53]]. The other three points we come back to once we have described the counterpropagating Rossby wave mechanism.

B. The counterpropagating Rossby wave mechanism

A kinematic/mechanistic interpretation of baroclinic instability is normally given in terms of a pair of counterpropagating Rossby edge waves (e.g., [59–61]) (although the concept of instability arising from a constructive interference of edge waves appears to hold for general shear instabilities, e.g., [68–72]). The mechanism is illustrated in Fig. 1(a) for the standard Eady problem [12] and proceeds as follows:

(1) Rossby waves are supported on potential vorticity gradients, and in the Eady setup, potential vorticity is only nonzero and localized at the upper and lower boundaries associated with buoyancy anomalies (e.g., [1]), and are thus vertically trapped Rossby edge waves.

(2) Rossby edge waves lead to potential vorticity anomalies, and these local potential vorticity anomalies induce a nonlocal velocity (via potential vorticity inversion; cf. [60]), such that the edge waves are individually *counter* propagating against the background mean flow.

(3) Edge waves can influence each other via the induced nonlocal velocity, and depending on the associated *phase shift* between the edge wave pairs, can lead to mutual amplification/damping of the edge wave displacement, as well as some hindering/helping of the other edge wave's propagation [60,61]:

(i) Taking the edge-wave *phase shift* $\Delta\epsilon$ to be measured in terms of potential vorticity anomalies relative to the lower wave, $\Delta\epsilon \in (0, \pi)$ will lead to constructive interference (the theoretical optimum being a quarter of a wavelength or $\pi/2$ out of phase, as illustrated in Fig. 1(a), and destructive interference for $\Delta\epsilon \in (-\pi, 0)$.

(ii) On the other hand, the waves are helping each other's propagation if $\Delta\epsilon \in (-\pi/2, \pi/2)$ (where they are maximally helping at $\Delta\epsilon = 0$ [cf. Fig. 1(a)] but where the induced vertically pointing velocity arrows will line up with each other), and hindering for $\Delta\epsilon \in [-\pi, -\pi/2) \cup (\pi/2, \pi]$ (maximally hindering at $\Delta\epsilon = \pm\pi$).

(4) The counterpropagation against the mean flow and the hindering/helping from the mutual edge-wave interaction can lead to a phase-locked configuration, and if the phase shift is such that we have constructive interference, then we have (modal) instability.

With this description for instability, we would perhaps expect certain features in the associated instability eigenfunction. For the edge-wave schematic given in Fig. 1(a), we would suspect, for example, that the instability eigenfunction should have a potential vorticity signature that tilts *into* the shear. For the Eady problem, the instability eigenfunction should span the whole depth, i.e., *deep* modes, because the edge waves are trapped on the opposite vertical boundaries so the induced nonlocal velocity should be felt throughout the vertical domain (in contrast to say the Charney-Green problem where the modes are not deep, because the constituents are interior and boundary edge waves). In addition, we might suspect the eigenfunction associated with the most unstable mode might have a phase difference that is in line with the theoretical maximum of $\pi/2$, the case illustrated in Fig. 1(a), since that is the maximally constructively interfering case. We revisit these points in the next section.

If we start from the present description for instability, the presence of the bottom slope would modify the background potential vorticity gradient and thus the characteristics of the edge waves [cf. Fig. 1(b)]. The work of [43] alludes to this but stops short of elaborating on the details. The work of [53] goes slightly further by arguing that the edge-wave phase speeds would be different; in the setting as in Fig. 1(b), the bottom edge-wave would propagate *faster* (because the associated potential vorticity gradient is enhanced), and the associated Doppler-shifted velocity at the bottom $\overline{U}(z = -1) - c > 0$ must be smaller in value. In order to maintain phase locking, we would need the Doppler-sifted velocity at the top $\overline{U}(z = +1) - c$ to match the $\overline{U}(z = -1) - c > 0$. That can happen only if c *decreases* in value, which for Rossby waves means selecting a higher wave number, i.e., shorter waves, providing an explanation for the observed instability bandwidth at least in the $\delta < 0$ regime [see Fig. 2(a)].

We argue, however, the above explanation based on phase-speed matching is overly simplified and incomplete. It does not provide an explanation to the second, third, and fourth observations made in the previous subsection, that (1) $c_r^+ = c_r^- > 0$ for $\delta < 0$ (and vice versa for $\delta > 0$), (2) where instability switches off for $\delta \gtrsim 1$, and (3) that the instability does not monotonically go to the longest wavelength as the slope is increased in the $\delta > 0$ case. The work of [53] also does not provide an explanation for the growth rate behavior over parameter space (at least not explicitly). The reader would presumably have noticed that the phase-speed matching argument being related to "phase locking" is only one part of the counterpropagating Rossby wave mechanism: neither "counterpropagation" nor the "mutual interaction" (from the nonlocal induced velocity associated

with the local potential vorticity anomalies) has been invoked thus far. We essentially argue in the subsequent parts that "phase locking" results from the "mutual interaction" aspect and is part of the solution, and arguments ignoring the interaction are fundamentally overly simplified and incomplete.

III. CLARIFYING THE INSTABILITY MECHANISM IN TERMS OF ROSSBY EDGE WAVES

In the previous section, we have highlighted various features that we might be looking for when analyzing the instability. We note, however, that while the edge-wave mechanism is often invoked, most of the time the analysis of the instability focuses on the normal mode eigenfunction $\tilde{\psi}$, which is perhaps at odds with the fact that we want to talk about edge waves. In this section, we reformulate the modified Eady problem explicitly in terms of Rossby or potential vorticity edge waves and its interaction (rather than in the streamfunction eigenfunction) to explore quantitatively how the presence of the bottom slope modifies the counterpropagating Rossby wave mechanism. We further make a distinction between the *phase shift* $\Delta\epsilon$, which exclusively refers to the *edge waves*, and the *phase tilt* $\Delta\epsilon_{\text{eigen}}$, which exclusively refers to the *tilt* associated with the normal-mode eigenfunction. We will essentially be arguing that the latter is widely used but can be a misleading quantity, while the former is the physical quantity that is of direct dynamical relevance.

A. Edge-wave formulation in phase-amplitude variables

The streamfunction eigenfunction $\tilde{\psi}(z)$ as it stands is in general a tilted structure in space that could be regarded as a superposition of edge-wave structures, and the problem here is in the definition of an appropriate separation of the tilted eigenfunction into the constituent edge-wave structures. While there is a general approach for constructing the potential vorticity edge waves in terms of wave activity variables such as pseudomomentum and pseudoenergy (e.g., [18,61,72–74]), we do not need that amount of complexity here since the edge-wave locations are well defined for the present problem. For elucidation purposes we will derive the structure and governing equations explicitly.

Consider expressing the streamfunction eigenfunction $\tilde{\psi}(z)$ in terms of a linear superposition of untilted structures focused at the top and bottom boundary (subscript T and B, respectively) such that

$$\tilde{\psi} = \tilde{\psi}_T + \tilde{\psi}_B, \quad \tilde{q} = \tilde{q}_T + \tilde{q}_B, \tag{9}$$

where the tilde denotes functions that are z-dependent only. Assuming modal solutions as in (6), $\tilde{q}$ and $\tilde{\psi}$ are related via

$$\tilde{q} = -\mu^2\tilde{\psi} + \frac{\partial^2\tilde{\psi}}{\partial z^2}, \tag{10}$$

subject to the boundary conditions that

$$\left.\frac{\partial\tilde{\psi}_T}{\partial z}\right|_{z=-1} = 0, \quad \left.\frac{\partial\tilde{\psi}_B}{\partial z}\right|_{z=+1} = 0. \tag{11}$$

Denoting $\hat{\delta}$ as the Dirac δ function, if we take (abusing mathematical rigor somewhat)

$$\tilde{q}_B = \hat{q}_B(t)\hat{\delta}(z+1), \quad \tilde{q}_T = \hat{q}_T(t)\hat{\delta}(z-1), \tag{12}$$

i.e., potential vorticity anomaly of an edge wave is nonzero only at the associated locations, then either by manually constructing a solution (cf. [67]) or by noting that we are in effect looking for the Green's function associated with the one-dimensional Helmholtz operator [in Eq. (10)] subject to homogeneous von Neumann conditions [in Eq. (11)], for which solutions are documented (e.g., online Green's function libraries, with appropriate changes of variable), or otherwise, the relevant

solutions are

$$\tilde{\psi}_B = -\hat{q}_B \frac{\cosh \mu(1-z)}{\mu \sinh 2\mu}, \quad \tilde{\psi}_T = -\hat{q}_T \frac{\cosh \mu(1+z)}{\mu \sinh 2\mu}. \tag{13}$$

Note that, with (13),

$$\tilde{b} = \frac{\partial \tilde{\psi}}{\partial z} = \begin{cases} -\hat{q}_T, & z = +1, \\ +\hat{q}_B, & z = -1, \end{cases} \tag{14}$$

demonstrating the explicit relation between buoyancy and potential vorticity anomalies, and that the top edge wave induces no potential vorticity anomaly at the location of the other edge wave.

Taking $\hat{q}_T = T e^{i\epsilon_T}$ and $\hat{q}_B = B e^{i\epsilon_B}$, where the amplitudes T, B and the phases $\epsilon_{T,B}$ are real functions only of time, substituting (13) into the governing Eqs. (3b) and (3c) and considering the real and imaginary parts lead to

$$\frac{1}{T}\frac{\partial T}{\partial t} = +\frac{k}{\mu \sinh 2\mu}\frac{B}{T}\sin \Delta\epsilon, \tag{15a}$$

$$\frac{1}{B}\frac{\partial B}{\partial t} = -\frac{k(1-\delta)}{\mu \sinh 2\mu}\frac{T}{B}\sin \Delta\epsilon, \tag{15b}$$

$$-\frac{1}{k}\frac{\partial \epsilon_T}{\partial t} = +\left[1 - \frac{1}{\mu \sinh 2\mu}\left(\cosh 2\mu + \frac{B}{T}\cos \Delta\epsilon\right)\right], \tag{15c}$$

$$-\frac{1}{k}\frac{\partial \epsilon_B}{\partial t} = -\left[1 - \frac{(1-\delta)}{\mu \sinh 2\mu}\left(\cosh 2\mu - \frac{T}{B}\cos \Delta\epsilon\right)\right], \tag{15d}$$

where we define $\Delta\epsilon = \epsilon_T - \epsilon_B$ as the phase shift of the edge wave in terms of the potential vorticity signature, consistent with the convention used in Sec. II B; $\Delta\epsilon > 0$ means the top wave has a potential vorticity signature that is *lagging behind* the bottom wave potential vorticity signature [cf. Fig. 1(a)]. The set of equations is cast in a form that is more similar to Eq. (14) of [68] for the two-dimensional formulation of the Rayleigh shear profile problem, but is equivalent to Eq. (7) of [67] which considers the phase shift in terms of the buoyancy variable instead. Note that since $\tilde{\psi} \sim -\tilde{q}$, the phase shift applies also to the streamfunction; contrast this to $\tilde{v} = ik\tilde{\psi}$, which would be shifted by $\pi/2$, and $\tilde{b}$, which would be shifted instead by π. Here $k/(\mu \sinh 2\mu)$ plays the role of the interaction function (cf. e^{-k} in [68] for the Rayleigh profile in the barotropic setting). Taking the amplitudes T and B as positive without loss of generality, we note that we need $\Delta\epsilon \in (0, \pi)$ for growth of edge waves, consistent with the description in Sec. II B and what we know about baroclinic instability: an unstable mode has the potential vorticity, streamfunction, and meridional flow patterns leaning *against* the shear (top signal lagging bottom signal; see Fig. 4 for an example), while the buoyancy pattern leans *into* the shear, corresponding to a shift by π (e.g., [1]).

While there are four independent variables in Eq. (15), the equations depend only on the amplitude ratios and the phase shift, and could be considered a two-dimensional dynamical system. Following the notation of [68], we define the amplitude ratio as $\tan\gamma = T/B$. Noting then various trigonometric identities such as

$$\frac{B^2 - T^2}{B^2 + T^2} = \cos 2\gamma, \quad \frac{B^2 + T^2}{2BT} = \frac{1}{2\sin 2\gamma},$$

(15) takes the form

$$\frac{\partial \gamma}{\partial t} = \frac{k}{\mu \sinh 2\mu}\sin \Delta\epsilon(\cos 2\gamma + \delta \sin^2 \gamma), \tag{16a}$$

$$\frac{\partial \Delta\epsilon}{\partial t} = \frac{2k}{\mu \sinh 2\mu}\left[\left(1 - \frac{\delta}{2}\right)\cosh 2\mu - \mu \sinh 2\mu + \left(\frac{1}{\sin 2\gamma} - \frac{\delta}{2}\tan\gamma\right)\cos \Delta\epsilon\right]. \tag{16b}$$

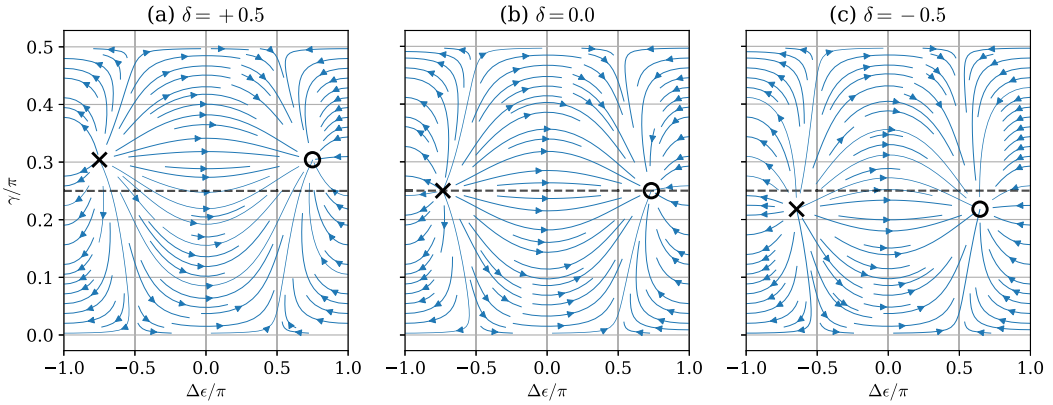

FIG. 3. Phase portrait and the fixed points of the dynamical system (stable and unstable mode marked on as a circle and cross respectively), for three choices of δ, at wave number $[k = k_{\max}(\delta),\, l = 0]$.

The set of equations should be compared with Eq. (15) of [68], noting the difference in the interaction function $[k/(\mu \sinh 2\mu)$ vs $\mathrm{e}^{-k}]$, arising from the differing physics between the systems being considered, encapsulated in the different Green's function of the associated system.

While the calculations are for general rescaled wave number μ, we will be focusing on the $l = 0$ (and $F = 1$) case as before. A dynamical system could be described in terms of phase portraits (e.g., [75]), and phase portraits associated with the most unstable wave number k for sample choices of δ are shown in Fig. 3. Note that the stable and unstable equilibrium points of the dynamical system (repellers and attractors) are associated with the unstable and stable normal modes, respectively, in the unstable bandwidth (cf. [61,68]). As the stability boundaries are passed there is a bifurcation, and the equilibrium points become centers located at $\gamma = 0, \pi/2$, and $\Delta\epsilon = \pm\pi$ (not shown), associated with neutral and freely propagating edge waves with no change in amplitude or phase. The nonequilibrium points have been argued to correspond to nonmodal growth (e.g., [67,68]), and the phase portraits indicate the regime transition in terms of edge waves edge waves as the nonmodal instabilities develop, but we leave this for a future study.

Focusing on the unstable modes (the attractors of the dynamical system), we note that the associated phase shifts $\Delta\epsilon$ is *not* $\pi/2$, even for the $\delta = 0$ case, which seems to contradict what is generally documented about the Eady problem having a phase shift of $\pi/2$ (e.g., [1]). There is in fact no discrepancy: taking the $\delta = 0$ case as an example (i.e., standard Eady problem), we compute the values of γ and $\Delta\epsilon$ associated with the stable equilibrium point and construct the edge-wave couplets as well as their sum, and these are shown in Fig. 4 (recalling $\hat{q} = B\mathrm{e}^{\mathrm{i}\epsilon_B}$, we take the reference to be $B = 1$ and $\epsilon_B = 0$). While $\Delta\epsilon \neq \pi/2$, their combination does lead to a phase tilt in the streamfunction eigenfunction $\Delta\epsilon_{\text{eigen}} = \epsilon(z = +1) - \epsilon(z = -1) = \pi/2$ (for an appropriately defined ϵ for the normal mode), and the reconstructed solution can be shown to coincide exactly with the one obtained from the more standard normal-mode analysis. A nonoptimal shift is realized simply because the mutual interaction from the interaction function (which is wave number dependent) is also part of the solution and provides extra *hindering* (since $\Delta\epsilon > \pi/2$; see Sec. II B) of the wave propagation required for phase locking (e.g., [61,62,68,71]). Considerations based simply on phase shift (or phase tilt) and/or phase-speed matching are overly simplified and incomplete, ignoring the interaction component, which is a fundamental part of the solution.

The statement in the above paragraph holds true for different values of k and δ (not shown). For synchronized growth of edge waves associated with stable equilibrium points of (16), we have $\Delta\epsilon \in (0, \pi)$ and $\gamma \in (0, \pi/2)$, so that the growth rate can be inferred from (15), given by

$$\sigma = \left| \frac{k}{\mu \sinh 2\mu} \frac{1}{\tan\gamma} \sin\Delta\epsilon \right| = \left| \frac{k(1-\delta)}{\mu \sinh 2\mu} \tan\gamma \sin\Delta\epsilon \right|, \tag{17}$$

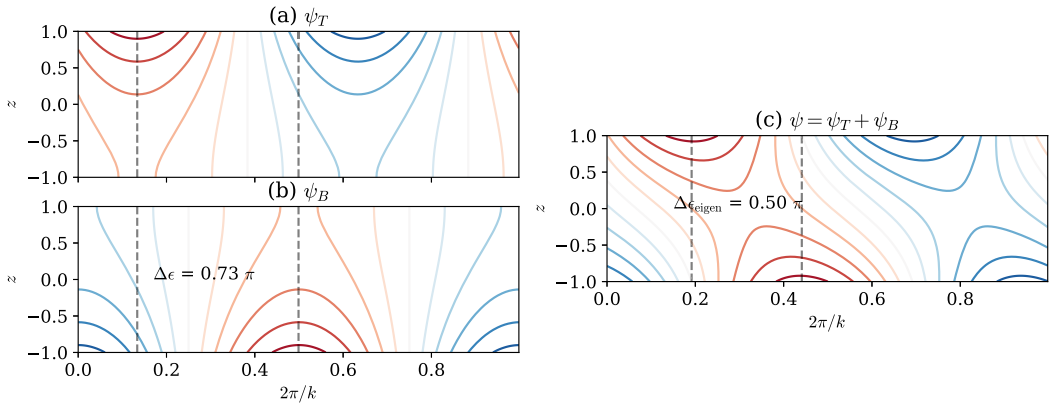

FIG. 4. Edge-wave components and the combination demonstrated for the most unstable mode of the standard Eady problem ($\delta = 0$). (a), (b) Associated edge-wave structure $\psi_{T,B}$ (referenced by $B = 1$ and $\epsilon_B = 0$) given in (13) of the attracting fixed point in Fig. 3(b), with $\Delta\epsilon \neq \pi/2$. (c) The reconstructed normal-mode $\psi = \psi_T + \psi_B$ that has a phase tilt $\Delta\epsilon_{\text{eigen}} = \pi/2$.

which numerically coincides with that of Fig. 2(a) (not shown). The phase speeds of the normal modes c_r can also in principle be reconstructed from the edge-wave basis via consideration of the self- and induced propagation by the edge waves (cf. [61,72]). The edge-wave formulation here encompasses the standard formulation of the modified Eady problem, which is not surprising given it is really a reformulation of the same problem, but expressing it in a form that allows for a mechanistic interpretation.

We show in Fig. 5 the amplitude ratios γ and edge-wave phase shift $\Delta\epsilon$ of equilibrium points of (16) associated with unstable modes (or attractors of the current dynamical system). Starting first with the amplitude ratio γ, it is clear that γ depends only on δ. The analytic expression for γ can be obtained by noting that, with synchronized growth and growth rate given by (17), we must have (with appropriate normalization and/or shifts in the phase)

$$\left|\frac{1}{\tan\gamma}\right| = \left|\frac{B}{T}\right| = \sqrt{1-\delta}, \tag{18}$$

which is k independent. Notice that:

(1) $|B/T|$ is ill-defined for $\delta > 1$, corresponding to the case where there is no instability (since there is no counterpropagation possible for the bottom wave as the bottom background potential vorticity gradient has switched signs)

(2) $|B| = 0$ for $\delta = 1$ for physically sound solutions (coinciding with vanishing potential vorticity gradient at the bottom)

(3) $|T| > |B|$ for $\delta \in (0, 1)$, i.e., weaker bottom wave

(4) $|T| = |B|$ for $\delta = 0$, and there is no asymmetry in the standard Eady case

(5) $|B| > |T|$ for $\delta < 0$, and there is *always* instability possible for $\delta < 0$.

The behavior of $\Delta\epsilon$ in Fig. 5(c) is in line with kinematic arguments given in Sec. II B. We generally need $\Delta\epsilon \in (0, \pi)$ for constructive interference. At fixed δ, long waves propagate faster (since these are Rossby edge waves), and the edge waves need to *hinder* each other to maintain phase locking, which for instability requires $\Delta\epsilon \in (\pi/2, \pi)$. The converse holds for shorter waves, requiring $\Delta\epsilon \in (0, \pi/2)$ (e.g., [61]), hence we would expect that, for fixed δ, as we move from small to large k through the unstable bandwidth, we obtain a transition a $\Delta\epsilon$ from π to 0, as seen in Fig. 5(c).

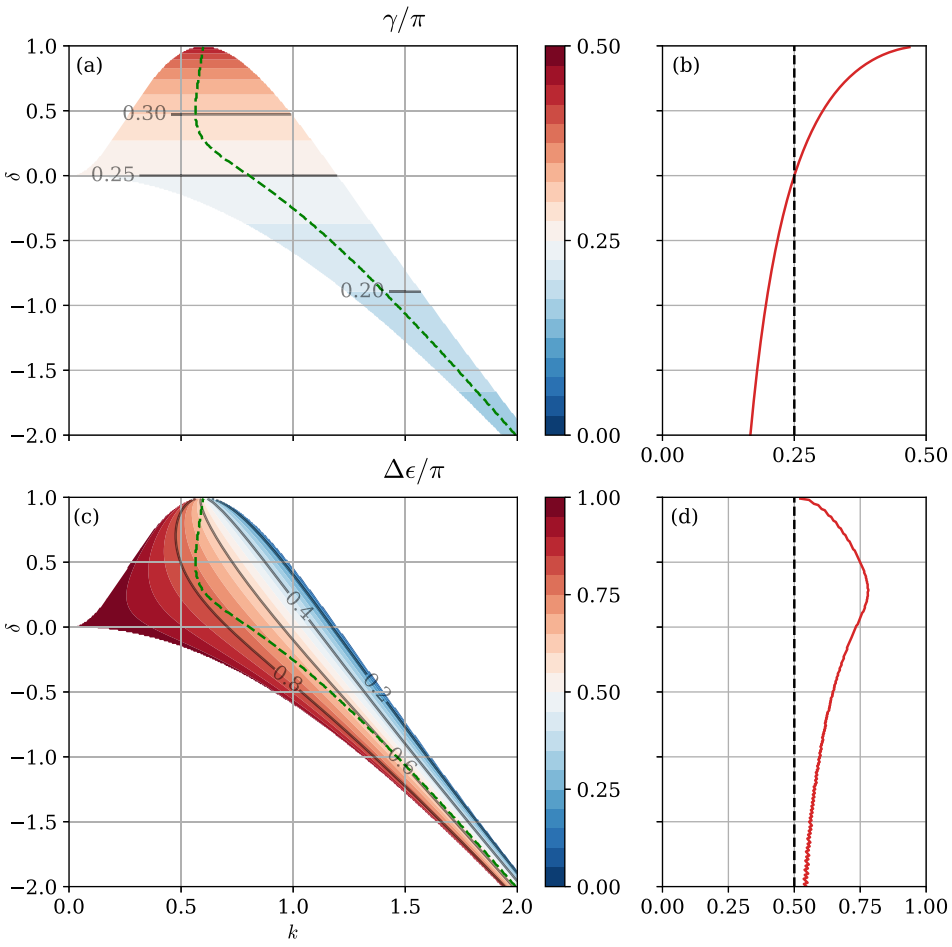

FIG. 5. (a) Normalized amplitude ratio γ in multiples of π as a function of k and δ (as shading and sample contours), and (b) the same quantity along the line of $k_{\max}(\delta)$ (red line); note 0.25 here denotes equal amplitude at top and bottom. (c) The normalized edge-wave phase shift $\Delta\epsilon$ in multiples of π as a function of k and δ (as shading and sample contours), and (d) the same quantity along the line of $k_{\max}(\delta)$ (red line); note $+0.5$ here denotes that the top edge wave *lags behind* the bottom edge wave by a quarter wavelength. The line of $k_{\max}(\delta)$ has been marked in panels (a) and (c) as the green dashed line.

B. Physical rationalization of the interacting edge-wave process

Our interpretation for the role of how the bottom sloping boundary modifies the counterpropagation Rossby wave mechanism is then as follows. Suppose we start at the location in (k, δ) parameter space of the most unstable mode of the classical Eady problem (with $\delta = 0$). At the same k but moving to $\delta < 0$, the bottom wave is strengthened and propagates faster, but also leads to a stronger induced velocity at the location of the top wave. The strong interaction leads to a stronger *hindering* effect, which will in general lead to a suboptimal phase-shift configuration. One way to drive the configuration towards a more optimal configuration would be to go towards *shorter* waves, offsetting the increased interaction [since the interaction function goes like $k/(\mu \sinh 2\mu)$ for the present Eady system]. This also then explains the reduction in the growth rate as we shift towards shorter waves [Fig. 2(a)]: while the efficiency could be adjusted via the phase shift, the interaction strength of the top wave on the bottom wave is *decreased*, so the net mutual interaction decreases. It would

seem that, in the $\delta < 0$ setting, it is *always* possible to compensate for the increase in interaction from increasingly negative δ by reducing the interaction function via increases in k, albeit over an increasingly narrow bandwidth of wave numbers. The phase speeds are positive [Fig. 2(b)] because the bottom edge wave propagating to the right (or eastwards) dominates over the top edge wave.

For the same thought experiment but moving to the $1 > \delta > 0$ regime, the bottom wave is weakened and leads to a weaker hindering effect in general. What this means is that the top wave is now propagating too fast, and this effect would have to be offset by increasing the interaction function via decreasing the wave number, i.e., going to longer wavelengths. The increase in the maximum growth rate for fixed $\delta > 0$ relative to the $\delta = 0$ setting is presumably related to the increases in the net mutual interaction from decreasing k [noting that there is no strong reason to expect the $\delta = 0$ case is in fact optimal for growth rates over the (k, δ) parameter space]. However, unlike the $\delta < 0$ case, reduction in k leads to an increase in edge-wave propagation since we are dealing with Rossby edge waves, and beyond a certain point it is simply not possible for the bottom wave's induced velocity and the background flow to hold the top wave into a phase-locked position, and instability is no longer possible. As $\delta \nearrow 1$, the potential vorticity gradient vanishes, counterpropagation is no longer possible, and no phase locking can be achieved. Note that $\delta \geqslant 1$ coincides with the nonsatisfaction of the Charney-Stern-Pedlosky condition that it is necessary for the background potential vorticity gradient to change sign in the domain in order for instability to occur. The phase speeds are negative [Fig. 2(c)] because the top edge wave propagating to the left (or westwards) dominates over the bottom edge wave.

C. Analysis in terms of the normal-mode eigenfunction

Here we provide an analogous analysis to demonstrate how different the results are if the instability streamfunction eigenfunction from (6) is utilized instead. Focusing on unstable modes, given a value of c, we can obtain the coefficients a and b for the vertical structure function $\tilde{\psi}(z)$ from (7). Given $\tilde{\psi}(z) = \tilde{\psi}_r + \mathrm{i}\tilde{\psi}_i$, we can compute for a (normalized) amplitude and phase of the eigenfunction via (e.g., [1,53])

$$|\tilde{\psi}(z)|^2 = \tilde{\psi}_r^2(z) + \tilde{\psi}_i^2(z), \quad \epsilon(z) = \arctan\frac{\tilde{\psi}_i(z)}{\tilde{\psi}_r(z)}. \tag{19}$$

Analogous to our edge-wave analysis in Sec. III, we introduce the quantities

$$\tan\gamma_{\text{eigen}} = \frac{|\tilde{\psi}(z=1)|}{|\tilde{\psi}(z=-1)|}, \quad \Delta\epsilon_{\text{eigen}} = \epsilon(z=1) - \epsilon(z=-1) \tag{20}$$

as a measure of the amplitude ratio and phase *tilt* (rather than phase shift) between the streamfunction eigenfunction at the top and bottom of the domain, respectively. Figure 6 shows the amplitude ratio γ_{eigen} and phase tilt $\Delta\epsilon_{\text{eigen}}$ as measured through the eigenfunction $\tilde{\psi}(z)$.

Starting first with the amplitude ratio, we note that the standard Eady case with $\delta = 0$ has $\gamma_{\text{eigen}} = \pi/4$ throughout the unstable bandwidth, i.e., the top and bottom of the normal mode have equal amplitude, and in fact the normal mode is symmetric about $z = 0$ for $\delta = 0$ (not shown; cf. [76]). For $\delta > 0$, $\gamma_{\text{eigen}} > \pi/4$, i.e., the normal-mode amplitude at the bottom is smaller than that at the top, and conversely for $\delta < 0$, consistent with results from physical expectations and edge-wave analysis. However, compared to the equivalent graph in terms of edge waves in Figs. 6(a) and 6(b), there is a wave-number dependence in γ_{eigen}, when our physical argument would suggest that the amplitude ratio should only depend on δ. The observation of γ_{eigen} is consistent if we remember that diagnosed quantities between two separate edge-wave structures do not necessarily need to be the same as that diagnosed from their combinations.

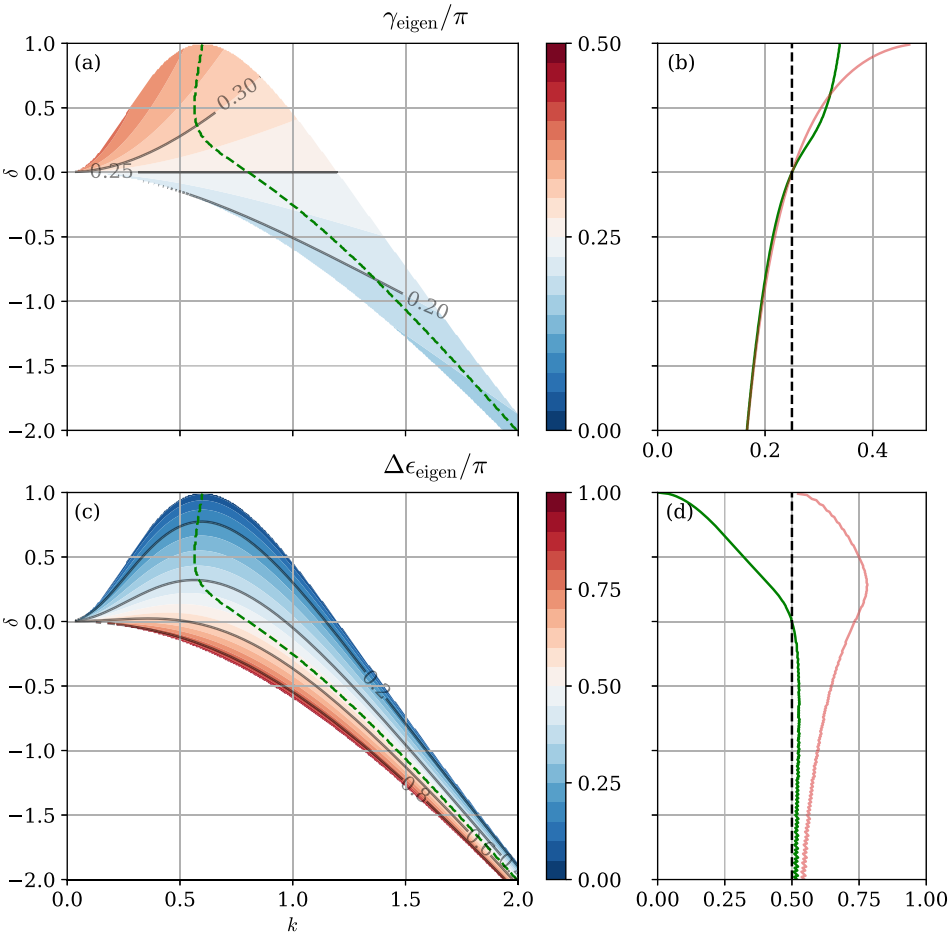

FIG. 6. Analog of Fig. 5 but for quantities diagnosed from the normal-mode directly. (a) Normalized amplitude ratio γ_{eigen} in units of π as a function of k and δ (as shading and sample contours), and (b) the same quantity along the line of $k_{\text{max}}(\delta)$ (green line, with γ from Fig. 5(b) as faint red line); note 0.25 here denotes equal amplitude at top and bottom. (c The normalized phase tilt in the streamfunction $\Delta\epsilon_{\text{eigen}}$ in units of π as a function of k and δ (as shading and sample contours), and (d) the same quantity along the line of $k_{\text{max}}(\delta)$ [green line, with $\Delta\epsilon$ from Fig. 5(d) as faint red line]; note $+0.5$ here denotes that the top edge wave *lags behind* the bottom edge wave by a quarter wavelength. The line of $k_{\text{max}}(\delta)$ marked in green has been marked in panels (a) and (c) as the green dashed line.

For the phase tilt in the streamfunction, in the standard Eady case with $\delta = 0$, the maximally growing mode has $\Delta\epsilon_{\text{eigen}} = \pi/2$, where the top signal lags behind the bottom signal by quarter of a wavelength. As the wave number increases, the tilt in the normal mode decreases, while the opposite is true as the wave number decreases. For $\delta \neq 0$, the behavior of $\Delta\epsilon_{\text{eigen}}$ in the streamfunction is asymmetric with the sign of δ. Notably, the most unstable wave number for $\delta < 0$ has $\Delta\epsilon_{\text{eigen}} = \pi/2$, indicating the most unstable mode is still able to access a standard Eady-like configuration in the normal mode, albeit with decreasing growth rate. However, while a phase shift of $\pi/2$ would be the optimum configuration for constructive interference in the edge-wave interaction framework (e.g., [60,61,67]), we should note that the phase shift $\Delta\epsilon$ need not coincide with the phase tilt $\Delta\epsilon_{\text{eigen}}$ [cf. Figs. 6(c) and 6(d) and Figs. 5(c) and 5(d)]. As was demonstrated in Fig. 4, $\Delta\epsilon$ is generally not at the expected optimal because one needs to take into account the interaction function. Additionally,

for fixed $\delta > 0$, the phase tilt does not have the transition from π to 0 over the unstable bandwidth as we would have expected from the physical arguments in Sec. II B for edge-wave interaction, further highlighting the unsuitability of using phase tilts when invoking the counterpropagating Rossby wave mechanism.

One could then wonder whether there is in fact any specific meaning to the value of the phase tilt $\Delta\epsilon_{\text{eigen}}$. It is certainly true that the phase tilt $\Delta\epsilon_{\text{eigen}}$ (as well as the edge-wave phase shift) should relate to an *energetic* interpretation of the instability (e.g., Sec. 6.7.2 of [1]), relating to the expectation that the fact that perturbations of meridional velocity v' and buoyancy b' should be overall positively correlated so that the zonally averaged meridional buoyancy flux $\overline{v'b'}$ is poleward, leading to a decrease in available potential energy. While the statement about the energetics is true, the problematic aspect is linking that to the raw value of $\Delta\epsilon_{\text{eigen}}$. Since in the linear instability analysis we should only be talking about rates and efficiencies, we might suspect that $\Delta\epsilon_{\text{eigen}} = \pi/2$ would correspond to maximum efficiency of the resulting $\overline{v'b'}$ in reducing available potential energy, i.e., maximum linear correlation. A straightforward linear regression analysis for the correlation of v' and b' over the whole spatial domain (not shown) indicates this is simply not true: v' and b' are maximally correlated in the linear sense at small k, and its dependence as a function of k and fixed δ bears no resemblance to $\Delta\epsilon_{\text{eigen}}$ or the growth rate plots (the scatter plots of v' against b' becomes increasingly "circular" with increasing k). The behavior of $\overline{v'b'}$ itself (making the choice of normalizing the eigenfunction $\tilde{\psi}(z)$ to have unit magnitude) also bears no resemblance to $\Delta\epsilon_{\text{eigen}}$ or the growth rate: for fixed δ, maximum $\overline{v'b'}$ occurs at a k larger than the wave number at which there is maximum growth (not shown). So while $\Delta\epsilon_{\text{eigen}}$ would in some way be related to the energetic as well as the kinematic/mechanistic view of the instability problem, it may perhaps be simpler to not attribute too much meaning to $\Delta\epsilon_{\text{eigen}}$; the fact that $\Delta\epsilon_{\text{eigen}} = \pi/2$ for the most unstable mode is curious and is perhaps worthy of further exploration.

IV. ANALYSIS IN THE GEOMETRIC FRAMEWORK

The previous section highlights subtleties when using the normal-mode eigenfunction for a mechanistic explanation, and argues that it is the edge waves that are more dynamically relevant. Does that mean the instability eigenfunctions have little utility relative to the edge waves? We provide a processing of the eigenfunctions in terms of the GEOMETRIC framework of [34,35] (see also [36,37]) that considers geometric quantities such as anisotropy factors and angles of eddy variance ellipses, and has been shown to have mechanistic links with shear instability (cf. the barotropic case, considered in [62]). The quantitative links between energetics and mechanistic interpretations are demonstrated here for a case where both the edge-wave couplet and eddy fluxes are well defined. The strong correlation of the geometric quantities with that diagnosed from the edge-wave framework provides a suggestion that, in cases where the edge waves are less well defined (e.g., the linear Charney-Green problem, or data from the nonlinear evolution of baroclinic instability), the GEOMETRIC framework may still be utilized and has energetic and dynamical relevance.

As a recap to the work of [34–36], in the quasigeostrophic limit, it is known that the eddy forcing on to the mean state is given by (e.g., [34])

$$\frac{\partial \overline{\boldsymbol{u}}}{\partial t} + f(\overline{\boldsymbol{u}}) = \nabla \cdot \mathbf{E}, \quad \mathbf{E} = \begin{pmatrix} -M+P & N & 0 \\ N & M+P & 0 \\ -S & R & 0 \end{pmatrix}, \tag{21}$$

where $\overline{\boldsymbol{u}}$ is the Reynolds averaged geostrophic flow, $f(\overline{\boldsymbol{u}})$ is some function, and $\mathbf{E}$ is the related to the Eliassen-Palm flux tensor that encodes all the eddy forcing onto the mean state. The entries in $\mathbf{E}$

can be written as

$$M = \frac{1}{2}\overline{v'^2 - u'^2} = -\gamma_m E \cos 2\phi_m \cos^2\lambda, \quad N = \overline{u'v'} = \gamma_m E \sin 2\phi_m \cos^2\lambda,$$
$$P = \frac{1}{2N_0}\overline{b'^2} = E\sin^2\lambda, \quad R = \frac{f_0}{N_0^2}\overline{u'b'} = \gamma_b \frac{f_0}{N_0} E \cos\phi_b \sin 2\lambda,$$
$$S = \frac{f_0}{N_0^2}\overline{v'b'} = \gamma_b \frac{f_0}{N_0} E \sin\phi_b \sin 2\lambda, \tag{22}$$

where the overbar denotes a mean operator (zonal average for the present work), M, N denote the eddy momentum fluxes (related to the Reynolds stresses), R, S denote the eddy buoyancy fluxes (related to the form stresses), P is the eddy potential energy, and $E = P + K$ is the total eddy energy, with the eddy kinetic energy K defined in the usual way. In this framework, the total eddy energy E becomes the only dimensional variable, which is arbitrary up to a multiplicative constant for the linear instability problem. By contrast, the nondimensional geometric quantities related to the eddy variance ellipses are independent of the arbitrary multiplicative constant, given by

$$\gamma_m = \frac{\sqrt{M^2 + N^2}}{K}, \quad \gamma_b = \frac{N_0}{2f_0}\sqrt{\frac{R^2 + S^2}{KP}},$$
$$\sin 2\phi_m = \frac{N}{\sqrt{M^2 + N^2}}, \quad \sin\phi_b = \frac{S}{\sqrt{R^2 + S^2}},$$
$$\frac{K}{E} = \cos^2\lambda, \quad \frac{P}{E} = \sin^2\lambda, \quad \tan^2\lambda = \frac{P}{K}, \tag{23}$$

where $\gamma_{m,b}$ are the momentum and buoyancy anisotropy parameters, $\phi_{m,b}$ are angle parameters related to the eddy momentum and buoyancy ellipses, while λ is an angle relating to the eddy energy partition. Note that there is a degeneracy in the angle parameters, where, for example, we could define ϕ_b in terms of $\cos\phi_b = R/\sqrt{R^2 + S^2}$ as in [34].

One idea relating to parametrization of eddy fluxes is that the nondimensional geometric parameters might be more universal and related to dynamics and/or instability characteristics compared to dimensional measures such as mixing lengths (which are system parameters), and so are perhaps be easier to parameterize. For example, it is known that in barotropic/horizontal shear instabilities, ϕ_m directly relates to the tilt angle of the eddy, and conversely (e.g., [34,36,37,62,77]). In the present modified Eady problem, it can be demonstrated that it is the eddy buoyancy rather than momentum fluxes that are the dominant contributions, consistent with the present setup leading to a pure baroclinic instability. The parameters of interest are then

$$\tan 2\phi_t = \gamma_b \tan 2\lambda, \quad \gamma_t = \frac{\cos 2\lambda}{\cos 2\phi_t}, \tag{24}$$

where ϕ_t and γ_t are the angle and anisotropy parameter of a vertical eddy in physical space [34,36,78]. From this, we note that we can define a nondimensional parameter α where

$$\alpha = \gamma_b \sin\phi_b \sin 2\lambda = \gamma_t \sin\phi_b \sin 2\phi_t. \tag{25}$$

The α parameter is a combination of geometric parameters that closely relates to the Eady growth rate, is bounded in magnitude by unity in the quasigeostrophic limit [34], and is one of the tuning parameters that is at present prescribed in parametrizations of baroclinic restratification effects (e.g., [39]). One interest here is on the dependence of ϕ_t and α on δ, namely, (1) how is the vertical eddy tilt angle ϕ_t linked with the edge phase shift $\Delta\epsilon$ or the normal mode phase shift $\Delta\epsilon_{\text{eigen}}$, and (2) what is the dominant contribution to the variation of α, with the possibility to aid/inform

our parametrization efforts for baroclinic eddies and its feedback onto the mean state in theoretical and/or numerical models (e.g., [39,79]).

Focusing again on the case of $l = 0$, i.e., no meridional variation, $u' = 0$, and so $R = N = 0$, while $M^2 = K$, and so

$$\gamma_m = 1, \quad \phi_m = 0, \quad \phi_b = \pm\frac{\pi}{2}, \quad \alpha = \pm\gamma_b \sin 2\lambda = \gamma_t \sin 2\phi_t. \tag{26}$$

For the present setup it is the sign of α that distinguishes whether we have instability or not, since ϕ_b is defined in term of the zonal mean meridional advection of eddy buoyancy fluxes S, and for instability we want a poleward flux of buoyancy with $S > 0$.

Figure 7 shows the value of the vertically averaged vertical tilt ϕ_t angle, α, and the buoyancy anisotropy γ_b over the unstable region in parameter space (note that the values are single-signed over depth). The vertical eddy angle ϕ_t has the behavior that $\phi_t \searrow 0$ as k is increased for fixed δ [Fig. 7(a)]. One interpretation of the tilt angle could be that it is related to $\Delta\epsilon$ of two interacting edge waves' phase shift leading to instability ($\phi_t = \pi/4$ might be expected to be analogous to a phase shift of $\Delta\epsilon = \pi/2$; cf. [62] for the case where the velocity shear is purely in the horizontal). Indeed, ϕ_t over parameter space as shown in Figs. 7(a) and 7(b) resembles that of $\Delta\epsilon$ over parameter space, as shown in Figs. 5(c) and 5(d). In that sense, even though ϕ_t is defined in terms of $S \sim \overline{v'b'}$ and makes no reference to edge-wave structures whatsoever, there are apparent mechanistic links of ϕ_t with $\Delta\epsilon$. In that regard, ϕ_t could perhaps serve as a possible proxy for edge-wave phase shifts that is easier to diagnose in cases where the definition of edge-wave structures becomes more ambiguous (e.g., dynamics in a nonlinear setting). Again, the phase tilt $\Delta\epsilon_{\text{eigen}}$ [Fig. 6(c)] bears little resemblance to ϕ_t [Fig. 7(a)] and $\Delta\epsilon$ [Fig. 5(e)] over parameter space.

It may be seen that α [Fig. 7(c)] correlates strongly with the growth rate [Fig. 2(a)], in line with the analysis of [34]. Although the values of α reported here are around an order of magnitude larger than what are used in parametrizations for numerical ocean models (e.g., [39]), we note that the diagnosed value here is for the linear instability analysis, while the values used in parameterizations are applied as averages over both energetic and quiescent regions and to mimic the feedback during the nonlinear phase. The sensitivity of α to δ is of most relevance, suggesting it should be α that is decreased in value in the presence of slopes particularly in the $\delta < 0$ scenario (where topographic and isentropic/isopycnal slopes are opposite in orientation), consistent with a previous diagnostic result in the nonlinear regime [56].

The dominant contribution to the variation of α (in both the average and pointwise sense) is principally through the buoyancy anisotropy parameter γ_b, as shown in Fig. 7(e). The eddy energy partition angle parameter λ plays a secondary role, since $\sin 2\lambda$ is diagnosed to be close to 1 in value in the pointwise sense (not shown). The presence of a sloping boundary would naturally be expected to force an anisotropy, and the feature of α correlating well with γ_b and not $\sin 2\lambda$ seems to be consistent with diagnoses from numerical simulations in a global ocean circulation model in the nonlinear regime [79], and diagnoses in the nonlinear regime of an idealized baroclinic flow over a topographic slope (personal communication with Huaiyu Wei and Yan Wang). The decreasing values of γ_b for fixed δ as k is increased corresponds to a statement in the previous section that the scatter plot of v' against b' becomes increasing "circular" in the same limit (cf. [34]). If we consider instead α in terms of ϕ_t and γ_t, then we see here that $\sin 2\phi_t$ would not correlate well with α, and neither would γ_t (not shown). So while there is a flexibility for the form of α used, it would seem that, in the linear regime at least, it is γ_b that is more relevant, and the presence of the slopes modifies the anisotropy of the state.

The diagnosed results above are presented as vertically averaged quantities, which does not demonstrate the asymmetry introduced with δ. Examination of the full vertical profiles does in fact show the quantities to be increasingly concentrated towards the lower boundary when $\delta < 0$ (and vice versa), consistent with the known behavior of γ in (18) and Fig. 5(a), the lower edge wave being the increasingly dominant (not shown).

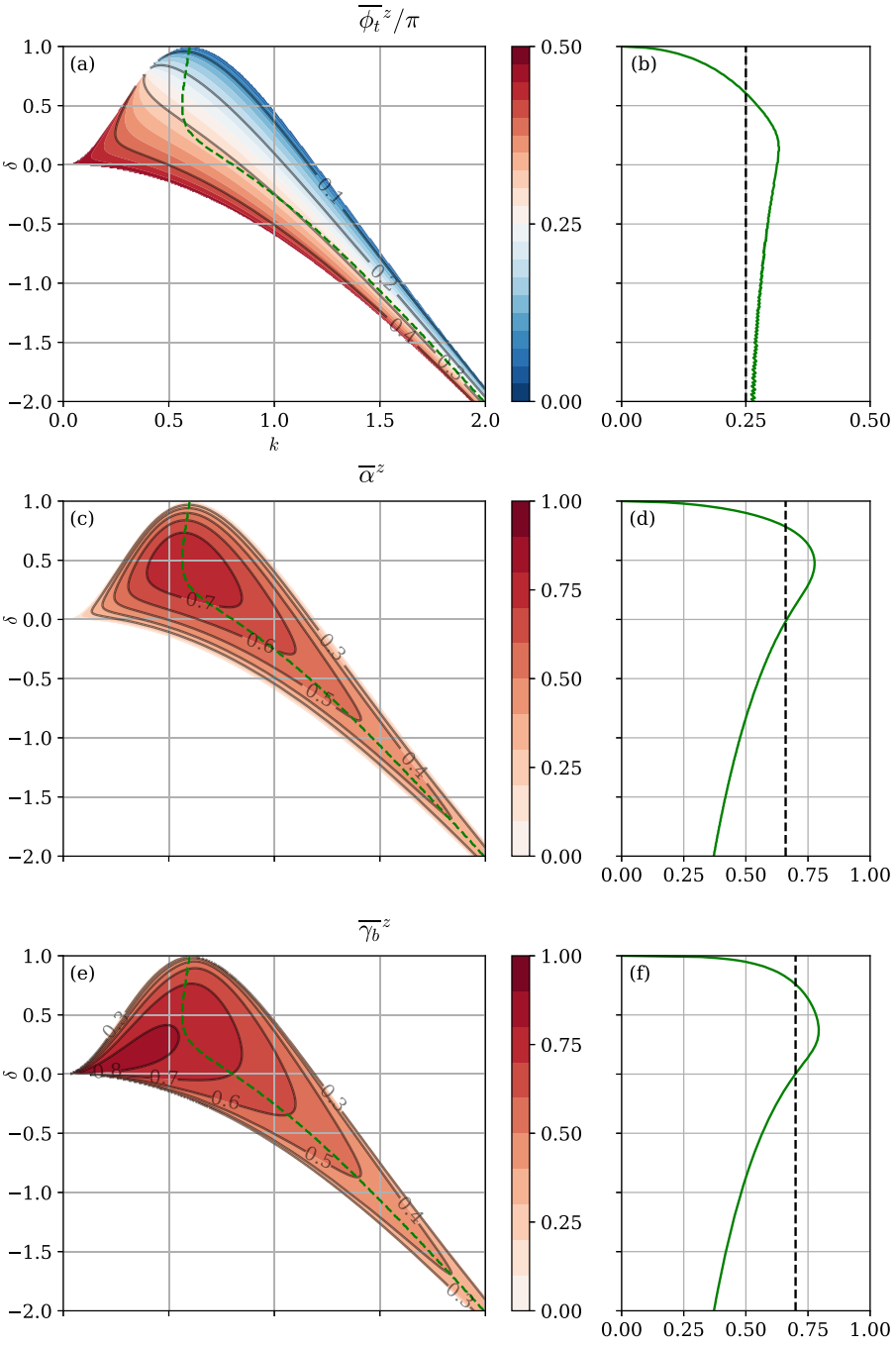

FIG. 7. Vertically averaged (a vertical eddy tilt angle $\overline{\phi_t}^z$ (in multiples of π), (c) $\overline{\alpha}^z = \overline{\gamma_b \sin 2\lambda}^z$, and (e) buoyancy anisotropy factor $\overline{\gamma_b}^z$ as a function of k and δ (as shading and sample contours), and (b), (d), (f) the respective quantities along the line of $k_{\max}(\delta)$. The line of $k_{\max}(\delta)$ marked in green has been marked in panels (a), (c), and (e) as the green dashed line.

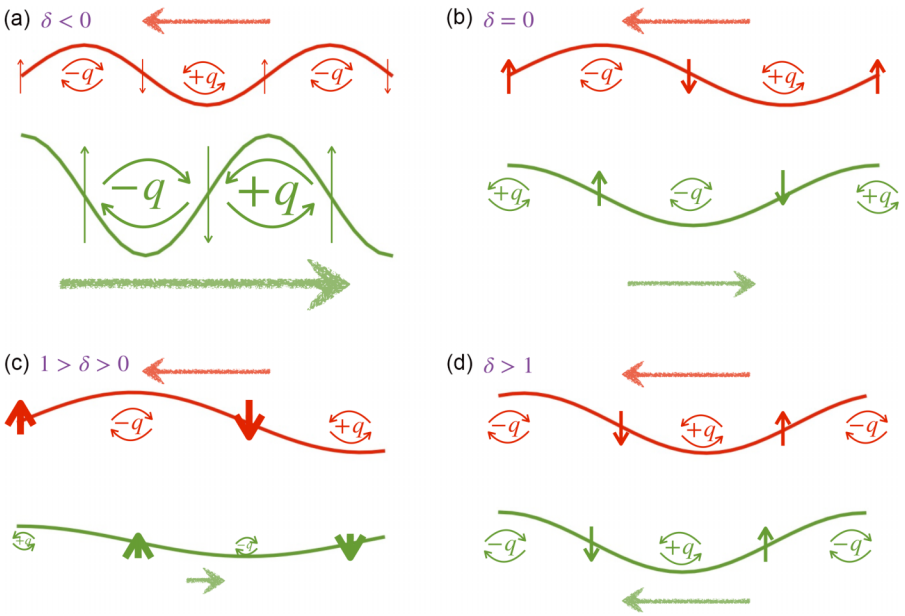

FIG. 8. Pictorial schematic for the change in instability characteristics over parameter space in terms of interacting Rossby edge waves, where longer arrows on the wave denotes the larger strength, and thicker arrows on the wave denotes a stronger action at a distance (weaker decay rate and more presence over the domain). (a) For the $\delta < 0$ case, the bottom potential vorticity gradient is stronger, leader to a stronger bottom edge wave that strengthens the magnitude of interaction and edge-wave propagation speed, but this effect can be compensated by going to shorter waves (thinner arrows on the waves). (b) The standard Eady case with $\delta = 0$, where the interaction is symmetric. (c) For $1 > \delta > 0$, the bottom potential vorticity gradient weakens, leading to a weaker bottom edge wave and a weaker interaction, but this can be offset somewhat by going to longer waves (thicker arrows on the waves). (d) For $\delta > 1$, the potential vorticity gradient switches sign and the bottom edge wave no longer counterpropagates against the background mean flow.

V. CONCLUSIONS AND DISCUSSION

The present work principally aims to clarify how the mechanism for baroclinic instability is modified over the presence of a bottom slope within the context of a modified Eady problem in the quasigeostrophic limit (cf. [41–45,53]). Previous works have argued that the changes in instability characteristics arise from changes in the edge-wave interaction, but these works consider only the need for phase-speed matching [47,53]. We argue that a rationalization based solely on phase-speed matching is overly simplified and incomplete, since the related arguments are not valid over all of parameter space, nor does it explain all the instability characteristics. Our explanation for the generation of baroclinic instability in terms of edge-wave interaction may be pictorially summarized as in Fig. 8, and is as follows:

(1) For $\delta < 0$, the bottom wave increases in strength, and not only does it intrinsically propagate faster (to the right or east), but leads to a larger action-at-a-distance via the larger induced velocity at the top wave. The increase in interaction can be compensated by reducing the vertical interaction function via moving to larger wave numbers (which also reduces the intrinsic propagation speed of both edge waves), and the weaker interaction function leads to weaker growth rates, since the top wave now influences the bottom wave less. It seems that it is always possible for such a compensation to be achieved in the $\delta < 0$ case, albeit over a decreasing bandwidth. Even if we have phase locking, since the bottom wave dominates, the instability might be expected to propagate to the right or east, i.e., the bottom wave drags the top wave with it in a phase-locked

configuration, which is consistent with the observation that $c_r^{\pm}(\delta < 0) > c_r^{\pm}(\delta = 0) = 0$ in our setting; see Fig. 2(c).

(2) For $\delta = 0$ (the standard Eady problem) we have the standard description for the counterpropagating Rossby wave mechanism. The interaction is symmetric, and we have $c_r^{\pm}(\delta = 0) = 0$ for our choice of basic state; see Fig. 2(e). It should be noted that a symmetric interaction does not necessarily imply the largest growth rates, since the interaction function also plays a role alongside the phase shift.

(3) For $\delta > 0$, the converse to the $\delta < 0$ case is true, except that the reduction in interaction from the weakened bottom wave cannot be arbitrarily increased by moving to smaller wave numbers, since that increases the intrinsic propagation speed of both edge waves. Decreases in wave number lead to increases in interaction [see Eq. (16), the $k/(\mu \sinh 2\mu)$ term], providing one explanation for why the maximum growth rate in (k, δ) parameter space occurs in the $\delta > 0$ regime. As $\delta \nearrow 1$, the top edge wave will become too fast with decreasing k, and the instability bandwidth decreases in width and shifted away from the small wave numbers. In this case, it is the top wave that dominates, and the instability might be expected to propagate to the left or west, i.e., the top wave drags the bottom wave with it in a phase-locked configuration, which is consistent with the observation that $c_r^{\pm} < c_r^{\pm}(\delta = 0) = 0$ in our setting; see Fig. 2(g).

(4) At $\delta \geqslant 1$ there is no instability since the potential vorticity gradient vanishes or reverses sign. There is no longer counterpropagation of the edge waves against the mean flow; see Fig. 1(b), where $\partial \overline{Q}_{\text{bot}}/\partial y > 0$ for sufficiently positive $\partial H_b/\partial y$.

The asymmetry is supported by the resulting edge-wave analysis, where the amplitude ratios are simply functions of δ independent of the wave number [Fig. 5(a)], consistent with the physical argument that δ modifies the background potential vorticity gradient at the bottom and should not have a wave number dependence; the analogous dependency is not seen in the amplitude ratios of the tilted normal-mode eigenfunction [Fig. 6(a)]. The point we want to emphasize here is that it is the asymmetry in the edge-wave amplitudes that lead to changes in the mutual interaction, that in turn modifies the phase-locking configuration, and the end result dictates a change in the phase shift. An argument based solely on phase-speed matching is by construction incomplete and overly simplified, since it neglects the interaction, which is a fundamental part of the solution. The physical rationalization applies generically to baroclinic instability over slopes; sample analysis on the analogous Phillips problem (cf. [45]) shows similar results and interpretations to here (not shown).

Noting that while the counterpropagating Rossby wave mechanism in terms of vertically trapped edge waves is often invoked, it is often that evidence relating to the normal-mode full-depth eigenfunction is presented instead, so for this work we provide an equivalent formulation of the modified Eady problem explicitly in terms of the edge waves (cf. [61,67,72]). The resulting problem is provided in terms of amplitude ratios γ and edge-wave phase shifts $\Delta\epsilon$, and the standard modal instability problem is effectively one of finding fixed points of a two-dimensional dynamical system. It is argued here that the edge-wave phase shift is the dynamically relevant quantity, while the normal-mode phase *tilt* $\Delta\epsilon_{\text{eigen}}$ can be misleading. Further analysis of the instability problem based on the GEOMETRIC framework [34] via diagnosing geometric parameters of the eddy variance ellipses (e.g., [36,62]) illustrates that there are strong correlations between the vertical eddy tilt angle ϕ_t and the edge-wave phase shift $\Delta\epsilon$ (cf. [62] for the analogous results for horizontal shear instability), and neither resemble the normal-mode phase tilt $\Delta\epsilon_{\text{eigen}}$.

One observation is that the phase shift of the edge waves $\Delta\epsilon$ associated with the most unstable mode is not necessarily at the theoretical optimum of $\pi/2$ (actually slightly larger, so that two edge waves hinder each other), while the phase *tilt* in the unstable streamfunction $\Delta\epsilon_{\text{eigen}}$ does seem to be at $\pi/2$ for $\delta \leqslant 0$. While we have no particularly convincing explanation as to the physical meaning (if any) of $\Delta\epsilon_{\text{eigen}} = \pi/2$, our analysis suggests that the phase shift $\Delta\epsilon$ should be the quantity of interest if a kinematic/mechanistic interpretation is to be invoked. The unstable normal mode is a linear combination of the edge-wave structures (e.g., Fig. 4), and the phase shifts in the untilted

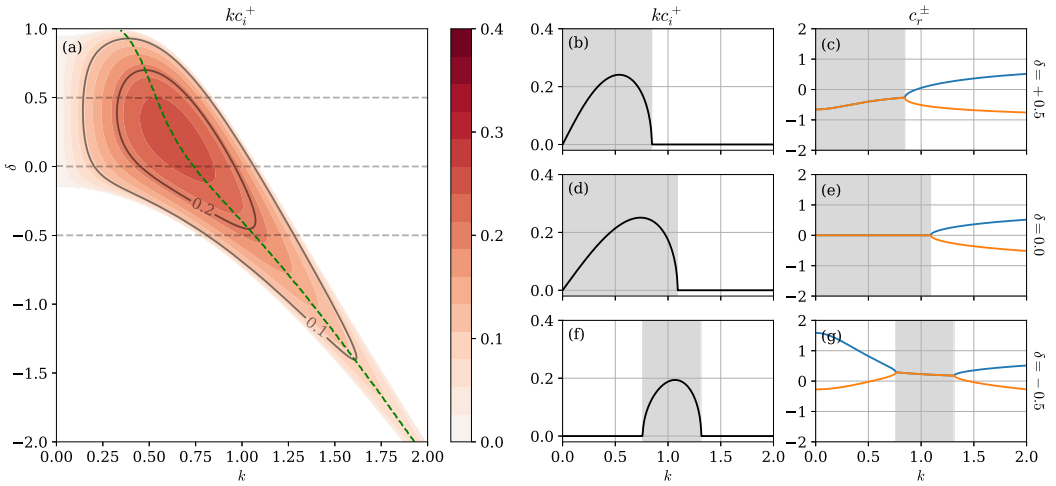

FIG. 9. Sample instability characteristics for $l = 0.5$, with the nontrivial meridional structure function $g(y) = \sin(y/2)$. (a) Growth rate as a function of the nondimensional wave number k and δ parameter (as shading and sample contours), and the green dashed line denoting $k_{\max}(\delta)$ where the growth rate is maximized. Also shown are the growth rates kc_i^+ and phase speed $c_r^\pm$ for (b), (c) $\delta = +0.5$, (d), (e) the standard Eady problem $\delta = 0.0$, and (f), (g) $\delta = -0.5$. The shaded regions in panels (b)–(g) denote the regions where there the growth rates are nonzero.

edge wave structures do not have to correspond to the phase tilts in the tilted streamfunction eigenfunctions. Given the results from the analysis performed in this work, we are of the opinion that references to $\Delta\epsilon_{\text{eigen}}$ should generally be avoided (an exception perhaps for the Phillips problem [13], where the entries of the normal modes are defined as per-layer quantities and could be argued to already be in edge-wave form).

Relating to the GEOMETRIC framework, beyond the link between the vertical eddy tilt ϕ_t and the edge-wave phase shifts $\Delta\epsilon$, we further explored the behavior of the α parameter from a linear instability point of view, to supplement parametrization efforts of relevance to ocean modeling. We find that there is a strong correlation of α with the instability growth rate over parameter space, and there is a suppression of α in the presence of slopes in the $\delta < 0$ regime. The dominant contribution to suppression of α comes from changes in the buoyancy anisotropy γ_b parameter (cf. [80]). The result here would be somewhat consistent with previous observations that buoyancy fluxes are suppressed over sloped regions (e.g., [43,44,46,48–53,55]), and that α is suppressed over slopes [56,79]. This work thus provides a consistency rationalization for the eddy parametrization proposal of [56], which was empirical in nature. The caveat is of course that diagnoses here are in the linear regime, and there is no strong reason theoretically that a linear instability analysis should remain valid in the nonlinear regime, although previous works have suggested that the linear instability characteristics can be useful in informing parametrizations that are invoked for the nonlinear regime (e.g., [29–33]). In the present case the diagnosed α is positive throughout the whole domain for an unstable mode in the Eady model for all cases that we have investigated. It remains an open question whether α may be related to the necessary criteria for instability (e.g., α only needs to be positive somewhere in the domain for the instability), but this question is beyond the scope of the present work (the Charney-Green problem [11,14] might be a more suitable setting to investigate that question).

Although the present work focuses largely on the zero meridional wave-number case $l = 0$, the results and observations apply to the $l \neq 0$ case. As a demonstration, the instability characteristics of $l = 0.5$ with the meridional structure function $g(y) = \sin(ly)$ are shown in Fig. 9. Here the instabilities generally possess weaker growth rates, with a change in the domain of instability in the

$\delta > 0$ region, but otherwise the general behavior of the growth rates and phase speed $c_r^{\pm}$ are similar to what has been reported. The physical rationalization in terms of edge waves is still applicable. The reduction in growth rates can be attributed to weakened interaction from $l \neq 0$, since that increases the value of $\mu = \sqrt{k^2 + l^2}/F$. The expanded domain of instability for $\delta > 0$ can be rationalized as edge waves having smaller intrinsic propagation speed in general (because of the increased μ), and so the top edge wave can be held in a phase-locking configuration for the given basic flow, and the weakened interaction associated with weaker bottom edge wave can in fact be compensated by increasing the interaction via decreasing the zonal wave number k. Edge-wave amplitude ratio γ is as given by (18), and the edge-wave phase shift $\Delta\epsilon$ has similar behavior to that observed in Fig. 5(c) (not shown). While the computation of the geometric parameters is slightly more complex as the relevant geometric variables are now two-dimensional, the conclusions and interpretations are essentially the same, except that the dominant contribution to α now comes from $\gamma_b \sin \phi_b$ (since R is no longer trivial and so $\phi_b \neq \pm\pi/2$), but the energy partition contribution $\sin 2\lambda$ is still close to 1 and largely constant over the domain. In particular, the vertical eddy tilt ϕ_t follows the phase shift $\Delta\epsilon$ more so than the phase tilts $\Delta\epsilon_{\text{eigen}}$ (in terms of spatial distribution, average values down the center line, or domain-averaged values; not shown).

The link between the edge waves and the GEOMETRIC formalism is curious since GEOMETRIC makes no explicit reference to edge-wave structures with its construction, and is possibly useful for two reasons. For the present linear problem the edge waves are well defined, and Sec. III provides a manual construction of the edge waves (e.g., where one part of the edge-wave couplet has an untilted structure and no potential vorticity signal at the location of the other edge wave). There are settings where edge-wave structures are harder to define (e.g., instability in the presence of planetary β [11,14,62], the Rayleigh sheet problem in the presence of a magnetic field [71]), or cases where one might naturally expect linear theory to no longer play a dominant role (e.g., during a nonlinear evolution). While there are still ways to define edge waves, for example, making use of orthogonality in the wave activity quantities such as pseudomomentum and pseudoenergy (e.g., [18,61,72,73]), the suggestive link between edge-wave interaction with the GEOMETRIC framework suggests that we could diagnose the GEOMETRIC quantities instead. Taking it further, if a GEOMETRIC-based parameterization is utilized in an ocean general circulation model, one could, for example, have an instability informed parametrization (cf. [29–33]) where there is a reduced model for counterpropagating Rossby waves running alongside an ocean general circulation model, from which we have an evolution for phase shifts and the like, which by its correlation tells us the relevant GEOMETRIC parameters, which can then be used to update parameters such as α during the runtime, leading to a state-aware parametrization. More work likely needs to be done to solidify the link between counterpropagating Rossby wave mechanism and GEOMETRIC framework first (e.g., the Charney-Green model, which has been pointed to possibly be more relevant than the Eady model in certain oceanic settings [e.g., [43,46,50,52]], problems with smooth profiles and/or profiles containing multiple potential vorticity gradients such as jet profiles, and mixed barotropic-baroclinic problems [e.g., [81,82]]), and is a subject for further research.

A more theoretical link is that of the underlying symmetries of the shear instability problem with counterpropagating Rossby waves, and by corollary with the GEOMETRIC framework. The resulting modified Eady system was claimed in this work to be parity-time ($\mathcal{PT}$) symmetric (cf. [64–66,83]), a concept stemming from quantum field theory; we refer the reader to the Appendix for the full details. The concepts of instability (neutral modes, unstable modes, stability boundary) have strong links with the counterpropagating Rossby wave mechanism (no phase locking, phase locking, bifurcation points), but also with concepts in $\mathcal{PT}$ symmetry ($\mathcal{PT}$-symmetric, spontaneous breaking of $\mathcal{PT}$ symmetry, Krein collision at exception points). The existence of such links is curious, as these lead to other questions such as (1) what are the analogous links with the GEOMETRIC framework? (2) Other systems are known or can be constructed to have different discrete symmetries (charge-parity-time symmetries [66]), does the symmetry dictate the characteristics of the interacting edge waves? (3) Can interacting edge waves serve as classical toy models for quantum

systems? (4) Can related tools from quantum field theory be adapted to reveal properties of classical systems (e.g., stability conditions)? We have not attempted to explore the role of such discrete symmetries in the present work, but that is a line of research we are actively looking into, results of which will be reported in other publications.

ACKNOWLEDGMENTS

This work was supported by the the RGC General Research Fund 11308021. The Python Jupyter notebook used to generate and analyze data for the problem may be found at [84]. G.K. was supported by a post-doctoral funding through the Center for Ocean Research in Hong Kong and Macau, a joint research center between the Laoshan Laboratory and Hong Kong University of Science and Technology. E.Q.Y.O. is supported by the Australian Government Research Training Program 678 Scholarship (RTP) and the Australian Research Council Special 676 Research Initiative, Australian Centre for Excellence in Antarctic Science (ARC Project No. 677 SR200100008). J.M. would like to thank L. Yeow in relation to the discussion on $\mathcal{PT}$ symmetry in classical systems. We thank the two referees and the participants of the Theoretical and Practical Perspectives in Geophysical Fluid Dynamics program at the International Centre of Theoretical Sciences in Bangalore, India (ICTS/TAPGFD2024/05) for their various comments on the work and manuscript, which have lead to improvements of the technical and presentation aspects of the article.

Authorship is alphabetical after the first author. Resources, supervision, project administration, funding acquisition: J.M. Conceptualization, visualization: J.M., N.H., E.H.. Methodology: J.M., E.H., G.K. Software: J.M., G.K. Formal analysis: J.M., N.H., E.H., G.K.. Writing–original draft: J.M., N.H., E.H. Validation, writing–review and editing: everyone.

APPENDIX: PARITY-TIME ($\mathcal{PT}$) SYMMETRY OF THE MODIFIED EADY PROBLEM

In the main text we made the observation that Eq. (3) is invariant under the transformation

$$\mathcal{P} : (x, y) \mapsto (-x, -y), \quad \mathcal{T} : (t, \psi) \mapsto (-t, -\psi). \tag{A1}$$

More formally, an operator $\mathcal{H}$ governing a system is parity-time ($\mathcal{PT}$) symmetric if it satisfies

$$(\mathcal{PT})\mathcal{H}^*(\mathcal{PT})^{-1} = \mathcal{H}, \tag{A2}$$

where $\mathcal{H}^*$ denotes the complex conjugate (rather than the Hermitian conjugate $\mathcal{H}^\dagger$, which for a matrix representation involves a transpose on top of the element-wise complex conjugate).

$\mathcal{PT}$ symmetry is a concept that originates from quantum physics (e.g., [63]), but has found recent interest in classical fluid systems also (e.g., [64–66]). Here we show explicitly that the present modified Eady problem is $\mathcal{PT}$ symmetric, which leads to certain features in the solution spectrum that was previously highlighted in Sec. II. The ideas and tools were previous given in the work of [66] for the Phillips-like problem (two layer quasigeostrophic equations with uniform flow in each layer; cf. [1,13]). The following exposition is largely given for completeness, but also serves to highlight very suggestive links between $\mathcal{PT}$ symmetry, shear instability, and the counterpropagating Rossby wave formalism, possibly enabling tools to be borrowed from quantum physics to further our understanding of classical fluid systems (e.g., nonlinear shear instability), or providing classical analogs with well-understood physics to complement the mathematical analysis of quantum systems. The present fluid system could presumably be modified to imbue it with other discrete symmetries (cf. the Phillips problem in [66]), but this has not been explored here.

Note that we can write the linearized system (3) in the form

$$\frac{\partial}{\partial t}\mathcal{L}\varphi = \mathcal{M}\varphi, \tag{A3}$$

which is a generalized eigenvalue problem for the relevant operators $\mathcal{L}$ and $\mathcal{M}$ acting on an eigenfunction φ. If we are taking modal solutions as in (6), then $\mathcal{L}$ has an explicit representation

whose inverse that can in principle be computed for, and we can define $M = \mathcal{L}^{-1}\mathcal{M}$ where

$$c\phi = M\phi, \tag{A4}$$

with the eigenvector $\phi = (a, b)$ in this case. For the system here, it can be shown that (using again the notation $C = \cosh\mu$ and $S = \sinh\mu$)

$$L = \mu\begin{pmatrix} -S & C \\ S & C \end{pmatrix}, \quad L^{-1} = \frac{1}{2\mu CS}\begin{pmatrix} -C & C \\ S & S \end{pmatrix},$$
$$M = \frac{-1}{SC}\begin{pmatrix} \frac{\delta}{2\mu}C^2 & \left(1-\frac{\delta}{2}\right)\frac{CS}{\mu} - C^2 \\ \left(1-\frac{\delta}{2}\right)\frac{CS}{\mu} - S^2 & \frac{\delta}{2\mu}S^2 \end{pmatrix}, \tag{A5}$$

where L denotes the representation of $\mathcal{L}$ when modal solutions (6) are taken.

In the present work, M is already real, $\mathcal{PT}$ happens to be the negative identity in the matrix representation relevant for the present system [66], so M is $\mathcal{PT}$ symmetric. Another way to see that M is $\mathcal{PT}$ symmetric is to note that, for P and T denoting the matrix representations of $\mathcal{P}$ and $\mathcal{T}$, μ is invariant under $P : (k, l) \mapsto (-k, -l)$ (interpreting $\mu = |k|/F$ if $l = 0$), while T introduces a minus sign through its action on the eigenvector ϕ, but this is done twice, so since M is real, the above equality holds.

A particular consequence for M being $\mathcal{PT}$ symmetric is that the entries M are all real [which we have manually demonstrated here in (A5), but is in fact a general feature]. Further, the dispersion relation (A4), for a two-component system, satisfies

$$c^2 - \mathrm{Tr}(M) + \mathrm{Det}(M) = 0, \quad c = \tfrac{1}{2}[\mathrm{Tr}(M) \pm \sqrt{\mathrm{Tr}(M)^2 - 4\mathrm{Det}(M)}], \tag{A6}$$

where the trace and determinant of M are given by

$$M = \begin{pmatrix} a_1 & a_2 \\ a_3 & a_4 \end{pmatrix}, \quad \mathrm{Tr}(M) = a_1 + a_3, \quad \mathrm{Det}(M) = a_1a_4 - a_2a_3.$$

The entries of M are given in (A5), and the resulting dispersion relation and be shown to coincide exactly with that given (8) obtained from standard means. Further, the eigenfunction of the system (defined up to some arbitrary constant) can be written as

$$\phi = \begin{pmatrix} a \\ b \end{pmatrix} = \begin{pmatrix} a_2 \\ -a_1 + \frac{1}{2}\left(\mathrm{Tr}(M) \pm \sqrt{\mathrm{Tr}(M)^2 - 4\mathrm{Det}(M)}\right) \end{pmatrix}, \tag{A7}$$

and the eigenfunction ϕ is $\mathcal{PT}$ symmetric if ϕ is real. However, for the eigenvector of an unstable mode in the present system, $\mathrm{Tr}(M)^2 - 4\mathrm{Det}(M) < 0$, and the resulting eigenvector becomes complex and ceases being an eigenfunction of the $\mathcal{PT}$ operator (because there is an extra minus introduced under a complex conjugate of the eigenvector), and we have what is termed *spontaneous breaking of $\mathcal{PT}$ symmetry*. The boundaries between the region with and without spontaneous $\mathcal{PT}$ symmetry breaking are called *exceptional points*, and these correspond precisely to the locations of marginal stability. The collision of eigenvalues $c^{\pm}$ on the real axis into complex conjugates is related to what are known as *Krein collisions* (e.g., [63,65]).

It is perhaps easy to see that, using the same framework of [66], other shear flow instability problems should also be $\mathcal{PT}$ symmetric, such as Phillips-like problems (cf. [45,66]), Charney-Green-like problems (cf. [1,11,14]), the standard Rayleigh sheet problem [83] in hydrodynamics, the Rayleigh sheet problem in magnetohydrodynamics with a uniform background magnetic field (e.g., [71]), and more general shear flow problems presumably. Additionally, given the link between shear instabilities and its physical interpretation as a pair of interacting edge waves, one is left to wonder on the exact links between $\mathcal{PT}$ symmetry and interacting edge waves. Suggestive links include that spontaneous breaking of $\mathcal{PT}$ symmetry seems to correspond exactly to when phase locking occurs (cf. [66]). A Krein collision of the eigenvalue that occurs at exception points

requires opposite signed Krein signatures, reminiscent of the requirement that shear instabilities require modes of opposite signed wave activity to collide (as positive/negative energy modes [85] or pseudomomentum, e.g., [73]), which is sometimes interpreted as a necessary (but not sufficient) condition for instability is the need for counterpropagation of edge waves (e.g., [61]).

While an explicit link to the edge-wave system with $\mathcal{PT}$ symmetry has been highlighted in the recent work of [83], and low-dimensional edge-wave systems (low-dimensional in the sense of dynamical systems) could be considered as a rephrasing of certain shear instability problem (e.g., [61]), the links with the general shear instability problem for general shear flows remain to be explored (since generic shear flow instability problems should be regarded an infinite dimensional dynamical system). For example, what is the analog of the Krein signature of the modes of the governing operator in the more standard fluid dynamics context? (Likely something related to pseudomomentum or pseudoenergy?) How are the standard shear flow linear stability conditions related to the properties of the governing operator, and in terms of interacting edge waves? (Related to proofs of a purely real spectrum in $\mathcal{PT}$-symmetric systems, e.g., [86,87])? Are there conditions beyond the standard necessary but not sufficient conditions of shear instability derivable from the $\mathcal{PT}$-symmetry property, using techniques drawn from quantum physics? Most references of $\mathcal{PT}$ symmetry in relation to shear instability systems so far are on the linear problem, but are there nonlinear analogs of the stability conditions such as the Arnol'd conditions (e.g., [18]) derivable from a similar approach? Such links could in principle provide a mechanistic/physical interpretation to theoretical properties related to $\mathcal{PT}$ symmetry, and techniques in relation to analyzing $\mathcal{PT}$-symmetric systems from quantum physics could provide new approaches for improving our understanding of classical fluid/plasma systems. The role of $\mathcal{PT}$ symmetry for fluid/plasma systems remains to be fully explored.

[1] G. K. Vallis, *Atmospheric and Oceanic Fluid Dynamics* (Cambridge University Press, Cambridge, 2006).
[2] R. V. E. Lovelace, H. Li, S. A. Colgate, and A. F. Nelson, Rossby wave instability of Keplerian accretion disks, Astrophys. J. **513**, 805 (1999).
[3] Y. Kaspi and G. R. Flierl, Formation of jets by baroclinic instability on gas planet atmospheres, J. Atmos. Sci. **64**, 3177 (2007).
[4] D. W. Hughes, R. Rosner, and N. O. Weiss, *The Solar Tachocline* (Cambridge University Press, Cambridge, 2007).
[5] R. J. Teed, C. A. Jones, and R. Hollerbach, Rapidly rotating plane layer convection with zonal flow, Geophys. Astrophys. Fluid Dyn. **104**, 457 (2010).
[6] I. Polichtchouk and J. Y. Cho, Baroclinic instability on hot extrasolar planets, Mon. Not. R. Astron. Soc. **424**, 1307 (2012).
[7] P. A. Gilman and M. Dikpati, Baroclinic instability in the solar tachocline, Astrophys. J. **787**, 60 (1402).
[8] P. A. Gilman, Effect of toroidal fields on baroclinic instability in the solar tachocline, Astrophys. J. **801**, 22 (2015).
[9] P. Read, D. Kennedy, N. Lewis, H. Scolan, F. Tabataba-Vakili, Y. Wang, S. Wright, and R. Young, Baroclinic and barotropic instabilities in planetary atmospheres: Energetics, equilibration and adjustment, Nonlinear Processes Geophys. **27**, 147 (2020).
[10] R. Yellin-Bergovoy, O. M. Umurhan, and E. Heifetz, A minimal model for vertical shear instability in protoplanetary accretion disks, Geophys. Astrophys. Fluid Dyn. **115**, 674 (2021).
[11] J. G. Charney, Dynamics of long waves in a baroclinic westerly current, J. Meteor. **4**, 136 (1947).
[12] E. T. Eady, Long waves and cyclone waves, Tellus **1**, 33 (1949).
[13] N. A. Phillips, The general circulation of the atmosphere: A numerical experiment, Q. J. R. Meteorol. Soc. **82**, 123 (1956).
[14] J. S. A. Green, A problem in baroclinic instability, Q. J. R. Meteorol. Soc. **86**, 237 (1960).

[15] J. G. Charney and M. E. Stern, On the stability of internal baroclinic jets in a rotating atmosphere, J. Atmos. Sci. **19**, 159 (1962).
[16] J. Pedlosky, The stability of currents in the atmosphere and the ocean: Part I, J. Atmos. Sci. **21**, 201 (1964).
[17] J. Pedlosky, The stability of currents in the atmosphere and the ocean: Part II, J. Atmos. Sci. **21**, 342 (1964).
[18] T. G. Shepherd, Symmetries, conservation laws, and Hamiltonian structure in geophysical fluid dynamics, Adv. Geophys., 287 (1990).
[19] T. G. Shepherd, Nonlinear saturation of baroclinic instability: Part I: The two-layer model, J. Atmos. Sci. **45**, 2014 (1988).
[20] T. G. Shepherd, Nonlinear saturation of baroclinic instability: Part II: Continuous stratified fluid, J. Atmos. Sci. **46**, 888 (1989).
[21] C. D. Thorncroft, B. J. Hoskins, and M. E. McIntyre, Two paradigms of baroclinic-wave life-cycle behaviour, Q. J. R. Meteorol. Soc. **119**, 17 (1993).
[22] V. D. Larichev and I. M. Held, Eddy amplitudes and fluxes in a homogeneous model of fully developed baroclinic instability, J. Phys. Oceanogr. **25**, 2285 (1995).
[23] M. A. Spall and D. C. Chapman, On the efficiency of baroclinic eddy heat transport across narrow fronts, J. Phys. Oceanogr. **28**, 2275 (1998).
[24] A. F. Thompson and W. R. Young, Two-layer baroclinic eddy heat fluxes: Zonal flows and energy balance, J. Atmos. Sci. **64**, 3214 (2007).
[25] J. G. Esler, The turbulent equilibration of an unstable baroclinic jet, J. Fluid Mech. **599**, 241 (2008).
[26] S. D. Bachman and B. Fox-Kemper, Eddy parametrization challenge suite I: Eady spindown, Ocean Modell. **64**, 12 (2013).
[27] S. D. Bachman, D. P. Marshall, J. R. Maddison, and J. Mak, Evaluation of a scalar transport coefficient based on geometric constraints, Ocean Modell. **109**, 44 (2017).
[28] C. Chang and I. M. Held, A scaling theory for the diffusivity of poleward eddy heat transport based on Rhines scaling and the global entropy budget, J. Atmos. Sci. **79**, 1743 (2022).
[29] J. S. A. Green, Transfer properties of the large-scale eddies and the general circulation of the atmosphere, Q. J. R. Meteorol. Soc. **96**, 157 (1970).
[30] P. H. Stone, A simplified radiative-dynamical model for the static stability of rotating atmospheres, J. Atmos. Sci. **29**, 405 (1972).
[31] P. D. Killworth, On the parameterization of eddy transfer, Part I. Theory, J. Mar. Res. **55**, 1171 (1997).
[32] P. D. Killworth, On the parameterization of eddy transfer, Part II. Tests with a channel model, J. Mar. Res. **56**, 349 (1998).
[33] C. Eden, A closure for meso-scale eddy fluxes based on linear instability theory, Ocean Modell. **39**, 362 (2011).
[34] D. P. Marshall, J. R. Maddison, and P. S. Berloff, A framework for parameterizing eddy potential vorticity fluxes, J. Phys. Oceanogr. **42**, 539 (2012).
[35] J. R. Maddison and D. P. Marshall, The Eliassen–Palm flux tensor, J. Fluid Mech. **729**, 69 (2013).
[36] B. J. Hoskins, I. N. James, and G. H. White, The shape, propagation and mean-flow interaction of large-scale weather systems, J. Atmos. Sci. **40**, 1595 (1983).
[37] S. Waterman and B. J. Hoskins, Eddy shape, orientation, propagation, and mean flow feedback in western boundary current jets, J. Phys. Oceanogr. **43**, 1666 (2013).
[38] J. Mak, J. R. Maddison, D. P. Marshall, and D. R. Munday, Implementation of a geometrically informed and energetically constrained mesoscale eddy parameterization in an ocean circulation model, J. Phys. Oceanogr. **48**, 2363 (2018).
[39] J. Mak, D. P. Marshall, G. Madec, and J. R. Maddison, Acute sensitivity of global ocean circulation and heat content to eddy energy dissipation time-scale, Geophys. Res. Lett. **49**, e2021GL097259 (2022).
[40] J. Mak, J. R. Maddison, D. P. Marshall, X. Ruan, and Y. Wang, Scale-awareness in an eddy energy constrained mesoscale eddy parameterization, J. Adv. Model. Earth. Syst. **15**, e2023MS003886 (2023).
[41] S. K. Blumsack and P. Gierasch, Mars: The effects of topography on baroclinic instability, J. Atmos. Sci. **29**, 1081 (1972).

[42] C. R. Mechoso, Baroclinic instability of flows along sloping boundaries, J. Atmos. Sci. **37**, 1393 (1980).
[43] P. E. Isachsen, Baroclinic instability and eddy tracer transport across sloping bottom topography: How well does a modified Eady model do in primitive equation simulations? Ocean Modell. **39**, 183 (2011).
[44] K. Brink, Baroclinic instability of an idealized tidal mixing front, J. Mar. Res. **70**, 661 (2012).
[45] C. Chen and I. Kamenkovich, Effects of topography on baroclinic instability, J. Phys. Oceanogr. **43**, 790 (2013).
[46] P. E. Isachsen, Baroclinic instability and the mesoscale eddy field around the Lofoten Basin, J. Geophys. Res. Oceans **120**, 2884 (2015).
[47] J. Pedlosky, Baroclinic instability over topography: Unstable at any wave number, J. Mar. Res. **74**, 1 (2016).
[48] G. E. Manucharyan, A. F. Thompson, and M. A. Spall, Eddy-memory mode of multi-decadal variability in residual-mean ocean circulations with application to the Beaufort Gyre, J. Phys. Oceanogr. **47**, 855 (2017).
[49] R. D. Hetland, Suppression of baroclinic instabilities in buoyancy-driven flow over sloping bathymetry, J. Phys. Oceanogr. **47**, 49 (2017).
[50] M. Trodahl and P. E. Isachsen, Topographic influence on baroclinic instability and the mesoscale eddy field in the northern North Atlantic Ocean and the Nordic seas, J. Phys. Oceanogr. **48**, 2593 (2018).
[51] Y. Wang and A. L. Stewart, Eddy dynamics over continental slopes under retrograde winds: Insights from a model inter-comparison, Ocean Modell. **121**, 1 (2018).
[52] G. E. Manucharyan and P. E. Isachsen, Critical role of continental slopes in halocline and eddy dynamics of the Ekman-driven Beaufort Gyre, J. Geophys. Res. Oceans **124**, 2679 (2019).
[53] S. Chen, C. Chen, and J. A. Lerczak, On baroclinic instability over continental shelves: Testing the utility of Eady-type models, J. Phys. Oceanogr. **50**, 3 (2020).
[54] Y. Tanaka, Stability of a flow over bottom topography: A general condition and a linear analysis in a two-layer quasi-geostrophic model with a possible application to a Kuroshio meander, J. Geophys. Res. Oceans **126**, e2021JC017849 (2021).
[55] H. Wei and Y. Wang, Full-depth scalings for isopycnal eddy mixing across continental slopes under upwelling-favorable winds, J. Adv. Model. Earth. Syst. **13**, e2021MS002498 (2021).
[56] H. Wei, Y. Wang, A. L. Stewart, and J. Mak, Scalings for eddy buoyancy fluxes across prograde shelf/slope fronts, J. Adv. Model. Earth. Syst. **14**, e2022MS003229 (2022).
[57] H. Wei, Y. Wang, and J. Mak, Parameterizing eddy buoyancy fluxes across prograde shelf/slope fronts using a slope-aware GEOMETRIC closure, J. Phys. Oceanogr. **54**, 359 (2024).
[58] A. Nummelin and P. E. Isachsen, Parameterizing mesoscale eddy buoyancy transport over sloping topography, J. Adv. Model. Earth Syst. **16**, e2023MS003806 (2024).
[59] F. P. Bretherton, Baroclinic instability and the short wavelength cut-off in terms of potential vorticity, Q. J. R. Meteorol. Soc. **92**, 335 (1966).
[60] B. J. Hoskins, M. E. McIntyre, and A. W. Robertson, On the use and significance of isentropic potential vorticity maps, Q. J. R. Meteorol. Soc. **111**, 877 (1985).
[61] E. Heifetz, C. H. Bishop, B. J. Hoskins, and J. Methven, The counter-propagating Rossby-wave perspective on baroclinic instability. I: Mathematical basis, Q. J. R. Meteorol. Soc. **130**, 211 (2004).
[62] T. Tamarin, J. R. Maddison, E. Heifetz, and D. P. Marshall, A geometric interpretation of eddy Reynolds stresses in barotropic ocean jets, J. Phys. Oceanogr. **46**, 2285 (2016).
[63] C. M. Bender, *PT Symmetry: In Quantum And Classical Physics*, 1st ed. (World Scientific, Singapore, 2018).
[64] H. Qin, R. Zhang, A. S. Glasser, and J. Xiao, Kelvin-Helmholtz instability is the result of parity-time symmetry breaking, Phys. Plasma **26**, 032102 (2019).
[65] R. Zhang, H. Qin, and J. Xiao, PT-symmetry entails pseudo-Hermiticity regardless of diagonalizability, J. Math. Phys. **61**, 012101 (2020).
[66] T. W. David, P. Delplace, and A. Venaille, How do discrete symmetries shape the stability of geophysical flows? Phys. Fluids **34**, 056605 (2022).
[67] H. C. Davies and C. H. Bishop, Eady edge waves and rapid development, J. Atmos. Sci. **51**, 1930 (1994).

[68] E. Heifetz, C. H. Bishop, and P. Alpert, Counter-propagating Rossby waves in the barotropic Rayleigh model of shear instability, Q. J. R. Meteorol. Soc. **125**, 2835 (1999).
[69] N. Harnik and E. Heifetz, Relating overreflection and wave geometry to the counter-propagating Rossby wave perspective: Toward a deeper mechanistic understanding of shear instability, J. Atmos. Sci. **64**, 2238 (2007).
[70] A. Rabinovich, O. M. Umurhan, N. Harnik, F. Lott, and E. Heifetz, Vorticity inversion and action-at-a-distance instability in stably stratified shear flow, J. Fluid Mech. **670**, 301 (2011).
[71] E. Heifetz, J. Mak, J. Nycander, and O. M. Umurhan, Interacting vorticity waves as an instability mechanism for magnetohydrodynamic shear instabilities, J. Fluid Mech. **767**, 199 (2015).
[72] E. Heifetz and A. Guha, Normal form of synchronization and resonance between vorticity waves in shear flow instability, Phys. Rev. E **100**, 043105 (2019).
[73] I. M. Held, Pseudomomentum and the orthogonality of modes in shear flows, J. Atmos. Sci. **42**, 2280 (1985).
[74] E. Heifetz, N. Harnik, and T. Tamarin, Canonical Hamiltonian representation of pseudoenergy in shear flows using counter-propagating Rossby waves, Q. J. R. Meteorol. Soc. **135**, 2161 (2009).
[75] S. H. Strogatz, *Nonlinear Dynamics and Chaos: With Applications to Physics, Biology, Chemistry, and Engineering (Studies in Nonlinearity)*, 1st ed. (CRC Press, Boca Raton, FL, 2000).
[76] N. Nakamura, Momentum flux, flow symmetry, and the nonlinear barotropic governor, J. Atmos. Sci. **50**, 2159 (1993).
[77] S. Waterman and J. M. Lilly, Geometric decomposition of eddy feedbacks in barotropic systems, J. Phys. Oceanogr. **45**, 1009 (2015).
[78] M. K. Youngs, A. F. Thompson, A. Lazar, and K. J. Richards, ACC meanders, energy transfer, and mixed barotropic–baroclinic instability, J. Phys. Oceanogr. **47**, 1291 (2017).
[79] M. B. Poulsen, M. Jochum, J. R. Maddison, D. P. Marshall, and R. Nuterman, A geometric interpretation of Southern Ocean eddy form stress, J. Phys. Oceanogr. **49**, 2553 (2019).
[80] K. D. Stewart, P. Spence, S. Waterman, J. Le Sommer, J.-M. Molines, J. M. Lilly, and M. H. England, Anisotropy of eddy variability in the global ocean, Ocean Modell. **95**, 53 (2015).
[81] I. N. James, Suppression of baroclinic instability in horizontally sheared flows, J. Atmos. Sci. **44**, 3710 (1987).
[82] N. Nakamura, An illustrative model of instabilities in meridionally and vertically sheared flows, J. Atmos. Sci. **50**, 357 (1993).
[83] C. Meng and Z. Guo, Vorticity wave interaction, Krein collision, and exceptional points in shear flow instabilities, Phys. Rev. E **108**, 065109 (2023).
[84] https://github.com/julianmak/julianmak.github.io/blob/master/files/Eady/Eady_analysis.ipynb
[85] R. A. Cairns, The role of negative energy waves in some instabilities of parallel flows, J. Fluid Mech. **92**, 1 (1979).
[86] P. Dorey, C. Dunning, and R. Tateo, Spectral equivalences, Bethe ansatz equations, and reality properties in PT-symmetric quantum mechanics, J. Phys. A: Math. Gen. **34**, 5679 (2001).
[87] A. Mostafazadeh, Pseudo-Hermiticity versus PT symmetry: The necessary condition for the reality of the spectrum of a non-Hermitian Hamiltonian, J. Math. Phys. **43**, 205 (2002).